MODELING AND OBSERVATIONS TO DETECT NEIGHBORHOOD-SCALE HEAT ISLANDS AND INFORM EFFECTIVE COUNTERMEASURES IN LOS ANGELES

A Report for:

California's Fourth Climate Change Assessment

Prepared By:

Haider Taha[1], George Ban-Weiss[2], Sharon Chen[3], Haley Gilbert[3], Howdy Goudey[3], Joseph Ko[2], Arash Mohegh[2], Angie Rodriguez[4], Jonathan Slack[3], Tianbo Tang[2], Ronnen Levinson[3]

[1]Altostratus Inc.
[2]University of Southern California
[3]Lawrence Berkeley National Laboratory
[4]National Autonomous University of Mexico

Edmund G. Brown, Jr., *Governor*

August 2018

CCCA4-CEC-2018-007

ACKNOWLEDGEMENTS

This work was funded by the California Energy Commission (CEC) under Agreement No. EPC-14- 073. Lawrence Berkeley National Laboratory was also supported by the Assistant Secretary for Energy Efficiency and Renewable Energy, Office of Building Technology, State, and Community Programs, of the U.S. Department of Energy under Contract No. DE-AC02-05CH11231.

We would like to acknowledge the support from our CEC Commission Agreement Manager, Susan Wilhelm, who has given us great latitude and guidance to overcome project hurdles. We were also very fortunate to have enlisted support from the Office of Mayor Eric Garcetti, City of Los Angeles; Los Angeles Unified School District (LAUSD); Los Angeles Department of Water and Power (LADWP); and Los Angeles Regional Collaborative, who have all been immensely supportive of this project. We wish to thank our Technical Advisory Committee members, Chris Weaver, U.S. Environmental Protection Agency; Robert Bornstein, San Jose State University; Ash Lashgari, California Air Resources Board; Bill Dean, California Environmental Protection Agency; Craig Tranby, LADWP; Tom Pyle, California Department of Transportation; Rupa Basu, California Environmental Protection Agency; and Henry Ortiz, LAUSD, for volunteering their time to provide us valuable feedback as we developed the research design.

We are grateful for Sabrina Bornstein, Jennifer Pope, Christopher Anyakwo, Marissa Aho, and Lauren Faber from the Office of Mayor Eric Garcetti, City of Los Angeles, who assisted us in connecting to and coordinating communications between the various City Departments to host stationary monitors. We want to thank Ming Gong, Greg Spotts, Mark Simon, Larry Hrezo, and Hugo Valencia from the Bureau of Street Services, City of Los Angeles for jumping at the opportunity to host a stationary monitor and helping us to install it. We also want to acknowledge the continued support from Craig Tranby at LADWP, who was a great resource for the duration of the project.

We wish to especially thank Marion Walsh, John Storie, Ronald Rackliffe, Jerry Lazzareschi, Henry Ortiz, Leslie Barret, and the principals and students of Sunny Brae and Melvin Elementary Schools, for hosting and assisting with the installation of two stationary monitors.

We also acknowledge Tom Vo from Southern California Association of Governments, the City of Los Angeles, and John Melvin from EarthDefine / CAL FIRE for providing high-resolution land-use and land-cover datasets. In addition, we are extremely grateful for the donated use of micrometeorological data from the WeatherBug network.

Jonathan Parfrey, of Climate Resolve; David Fink, formerly of Climate Resolve; Edith de Guzman, of Tree People; and Krista Kline and Zoe Elizabeth, each formerly of the Los Angeles Regional Collaborative, also were helpful during our search for suitable stationary monitor sites.

Lastly, we would like to acknowledge the assistance of many Uber drivers in the Los Angeles area who agreed to install our mobile measurement apparatus on their cars and drive along our transect routes.

PREFACE

California's Climate Change Assessments provide a scientific foundation for understanding climate-related vulnerability at the local scale and informing resilience actions. These Assessments contribute to the advancement of science-based policies, plans, and programs to promote effective climate leadership in California. In 2006, California released its First Climate Change Assessment, which shed light on the impacts of climate change on specific sectors in California and was instrumental in supporting the passage of the landmark legislation Assembly Bill 32 (Núñez, Chapter 488, Statutes of 2006), California's Global Warming Solutions Act. The Second Assessment concluded that adaptation is a crucial complement to reducing greenhouse gas emissions (2009), given that some changes to the climate are ongoing and inevitable, motivating and informing California's first Climate Adaptation Strategy released the same year. In 2012, California's Third Climate Change Assessment made substantial progress in projecting local impacts of climate change, investigating consequences to human and natural systems, and exploring barriers to adaptation.

Under the leadership of Governor Edmund G. Brown, Jr., a trio of state agencies jointly managed and supported California's Fourth Climate Change Assessment: California's Natural Resources Agency (CNRA), the Governor's Office of Planning and Research (OPR), and the California Energy Commission (Energy Commission). The Climate Action Team Research Working Group, through which more than 20 state agencies coordinate climate-related research, served as the steering committee, providing input for a multisector call for proposals, participating in selection of research teams, and offering technical guidance throughout the process.

California's Fourth Climate Change Assessment (Fourth Assessment) advances actionable science that serves the growing needs of state and local-level decision-makers from a variety of sectors. It includes research to develop rigorous, comprehensive climate change scenarios at a scale suitable for illuminating regional vulnerabilities and localized adaptation strategies in California; datasets and tools that improve integration of observed and projected knowledge about climate change into decision-making; and recommendations and information to directly inform vulnerability assessments and adaptation strategies for California's energy sector, water resources and management, oceans and coasts, forests, wildfires, agriculture, biodiversity and habitat, and public health.

The Fourth Assessment includes 44 technical reports to advance the scientific foundation for understanding climate-related risks and resilience options, nine regional reports plus an oceans and coast report to outline climate risks and adaptation options, reports on tribal and indigenous issues as well as climate justice, and a comprehensive statewide summary report. All research contributing to the Fourth Assessment was peer-reviewed to ensure scientific rigor and relevance to practitioners and stakeholders.

For the full suite of Fourth Assessment research products, please visit www.climateassessment.ca.gov. This report contributes to energy sector resilience by improving our understanding of factors that contribute to urban heat islands, which exacerbate peak energy demand, and by providing a basis for assessing the performance efforts to address urban heat islands.

ABSTRACT

To understand spatial air-temperature variations in local urban heat islands (UHIs) and urban cool islands (UCIs), and their relationship to land-use and land-cover (LULC) properties in the Los Angeles Basin, we sought to (a) use fine-resolution climate models to identify UHI / UCI areas, (b) relate observed intra-urban temperature variations (from mobile transects and stationary monitors) to LULC and surface physical properties, and (c) calibrate/validate the fine-resolution meso-urban climate models that were used in identifying the UHI / UCI. We conducted a multi-dimensional assessment of urban temperature variations based on numerical modeling and several types of observations, including mobile transects, dense networks of personal weather stations, and sparse but more accurate research-grade stationary weather monitors. To identify the causative factors of the UHI / UCI at the neighborhood scale, we collected detailed LULC datasets, such as 1-m (3.3 ft) resolution roof albedo and tree canopy cover, as inputs for the meteorological modeling and analysis. The fine-scale meteorological model was used to design mobile-transect routes and to site the stationary monitors based on the definition of UHI / UCI areas.

This study provides the first observational evidence from analysis of high spatial density weather stations that increases in roof albedo at neighborhood scale are associated with reductions in near-surface air temperature. This was corroborated with the analysis from mobile transect measurements and correlation of observed air temperature with neighborhood-scale albedo and vegetation canopy cover, which revealed a cooling effect from area-wide increase in albedo and/or canopy cover.

The calibrated meteorological model was able to accurately identify the localized UHIs / UCIs observed in this study. Interested stakeholders/researchers can use the same models and calibration / validation methodology to characterize the intra-urban microclimate variations elsewhere in California, and can apply them to analyze the benefits from deploying UHI countermeasures.

Keywords: Urban heat islands, urban cool islands, land-use and land-cover, intra-urban temperature variability, mobile transects, personal weather stations, stationary weather monitor, fine-scale meteorological model

Please use the following citation for this paper:

Taha, Haider, George Ban-Weiss, Sharon Chen, Haley Gilbert, Howdy Goudey, Joseph Ko, Arash Mohegh, Angie Rodriguez, Jonathan Slack, Tianbo Tang, Ronnen Levinson. (Lawrence Berkeley National Laboratory). 2018. ***Modeling and Observations to Detect Neighborhood-Scale Heat Islands and Inform Effective Countermeasures in Los Angeles.*** California's Fourth Climate Change Assessment, California Energy Commission. Publication Number: CCCA4-CEC-2018-007

HIGHLIGHTS

- Urban heat islands in California exacerbate peak energy demand and compromise public health in California. These impacts are intensified by climate change. Quantifying the factors that contribute to urban heat islands in California as well as the effectiveness of strategies to reduce the urban heat island effect contributes to climate resilience for the electricity sector and helps safeguard public health.
- In this study we carry out a multi-dimensional assessment of urban temperature variations in the Los Angeles Basin based on state-of-the-science numerical modeling and several types of observations, including mobile transects, dense networks of personal weather stations, and sparse but more accurate research-grade stationary weather monitors.
- Analysis of high spatial density weather stations provides, to our knowledge, the first observational evidence that increases in albedo (fraction of sunlight reflected) of roofs at neighborhood scale are associated with reductions in near-surface air temperature.
- Analysis of observed air temperature from mobile transects and their correlations with neighborhood-scale albedo and vegetation canopy cover shows a cooling effect from area-wide increase in albedo and/or canopy cover.
- In the San Fernando Valley study area, the largest localized heat islands were associated with lowest vegetation canopy cover; near downtown Los Angeles, areas with lower albedo caused the largest local heat islands.
- The calibrated meteorological model was found to reproduce accurately the intra-urban heat and cool islands observed in this study. Future projects will be able to use the same models and calibration / validation methodology to characterize the intra-urban microclimate variations elsewhere in California. The validated models will also enable the State to analyze urban heat island mitigation benefits in future efforts.
- A methodology was developed in this project to apply fine-scale meteorological modeling in siting weather stations and designing mobile-observation routes to monitor urban heat islands. The methodology was validated by comparing simulation results to observational micrometeorological data.
- The modeling developed here was used to determine ideal sites for new research-grade stationary weather monitors in the San Fernando Valley. Newly installed monitors can be used in assessments of urban heat islands and for tracking future temperatures. Monitor data can be accessed for free via Weather Underground:
    - Monitor_1: https://www.wunderground.com/personal-weather-station/dashboard?ID=KCACHATS19
    - Monitor_2: https://www.wunderground.com/personal-weather-station/dashboard?ID=KCAWINNE11
    - Monitor_3: https://www.wunderground.com/personal-weather-station/dashboard?ID=KCARESED8

TABLE OF CONTENTS

ACKNOWLEDGEMENTS ..... **i**

PREFACE ..... **ii**

ABSTRACT ..... **iii**

HIGHLIGHTS ..... **iv**

TABLE OF CONTENTS ..... **v**

1: Introduction **1**

2: Literature Review **2**

2.1 Modeling the Urban Heat Island Effect 2

2.2 Measurement of Urban Heat Islands 2

2.3 Effect of Land Use / Land Cover on Urban Heat Islands 2

3: Methodology **3**

3.1 Acquisition of External Weather Measurements 3

3.1.1 Criteria 4

3.1.2 Process 4

3.1.3 Quality Review 6

3.1.4 Datasets Selected 7

3.2 Study Area Identification 7

3.2.1 Characterization of Land Use / Land Cover (LULC) 7

3.2.2 Climate Modeling Results and Suggestions for Study Areas 10

3.2.3 Preliminary Mobile Transects to Select Areas 11

3.2.4 Study Areas Selected 11

3.3 Stationary Weather Measurement 15

3.3.1 Criteria 15

3.3.2 Monitor Design 15

3.3.3 Monitor Calibration 17

3.3.4 Stationary Monitor Installation 17

3.3.5 Monitor Operation 18

3.4 Mobile Observation Path Selection 18

3.5 Mobile Monitor Design and Operation 19
3.5.1 Design 19
3.5.2 Calibration 24
3.5.3 Operation 24
3.6 Calibration of climate model to observations 24
3.6.1 Description and Data Sources for Land Use Land Cover Properties Used in Personal Weather Station Analysis 28
4: Results and Discussion 30
4.1 Stationary Temperature Measurements 30
4.1.1 Deriving Sensitivities of Measured Air Temperature to LULC Properties 30
4.1.2 Spatial and Temporal Profiles 31
4.1.3 Relation to LULC 33
4.1.4 Utility of PWS Measurements 38
4.2 Mobile Temperature Measurements 38
4.2.1 Relation to LULC 38
4.3 Detection of Intra-urban Heat and Cool Islands 43
4.4 Performance and Utility of Mobile Monitors 43
5: Policy Implications and Lessons Learned 44
5.1 Lessons Learned 44
5.2 Policy Implications 44
6: Conclusions and Future Directions 45
6.1 Recommendations for Future Research 45
6.2 Conclusions 45
7: References 47

1: Introduction

Urban heat islands (UHIs) are categorized as either (a) skin-surface UHIs or (b) air-temperature UHIs. Air-temperature UHIs are relevant to building energy use, thermal comfort, public health, precursor emissions, air pollutant formation, and climate, and as such are the focus of this study. UHIs result in part from the transformation of urban land cover from trees and vegetation to buildings and other heat-absorbing urban infrastructure (Taha 1997; Pomerantz et al. 2000; Taha 2017).

Future climate change scenarios project that the annual number of extreme heat days in California's urban areas will increase. In the San Fernando Valley in the Los Angeles (LA) Basin, the number of extreme heat days (those with maximum air temperatures exceeding 39.7 °C [103.4 °F], based on the 98th percentile of daily maximum temperatures recorded April - October 1961 - 1990), are estimated to increase on average to 12 days per year from four by mid-century (Cal-Adapt 2018). Temperature increases induced by climate change would exacerbate existing heat islands, threatening human and non-human health and straining energy resources. While warming from climate change requires global action to mitigate, UHIs are city-specific phenomena with solutions a city can implement locally. UHI countermeasures, such as cool roofs and tree canopy cover, have been found in modeling studies to reduce urban temperatures when implemented at scale in cities (Santamouris 2014; Taha 2015; Taha 2008a-c).

To design and implement appropriate countermeasures, cities need to characterize urban heat and its causes (Taha 2013; Sailor et al. 2016). This project seeks to understand spatial variations in local heat and cool islands and their relationship to land-use and land-cover (LULC) properties, providing guidance for future mitigation via control measures such as higher albedo (solar reflectance) and more vegetation. The objective was to establish the causative factors of the local heat and cool islands at the neighborhood scale (Oke 1981; Grimmond 2006; Taha 1997) in the study areas, based on site-specific and upwind (a) micrometeorological dynamics (e.g., local generation of heat and transport of heat from upwind sources), (b) LULC properties, and (c) surface physical properties. We sought to (a) use fine-resolution climate models to identify UHI / Urban Cool Island (UCI) areas, (b) relate observed intra-urban temperature variations (from mobile transects and fixed weather stations) to LULC and surface physical properties, and (c) calibrate/validate the fine-resolution meso-urban climate models that were used in identifying the UHI / UCI. By understanding the variations in local heat and cool islands and their interaction with LULC properties, cities can implement policies to mitigate UHIs now and build resiliency to future urban warming from climate change.

To characterize the meteorological variables in the study areas, we collected data from existing weather networks; conducted detailed, fine resolution meteorological modeling; installed research-grade stationary weather monitors; and performed mobile transects. We partnered with the City of Los Angeles, County of Los Angeles, and Los Angeles Unified School District (LAUSD) to help us identify and host stationary monitors in two study areas that we identified: (1) "SFV5", an area that is part of the San Fernando Valley (SFV); and (2) "LA1", a region that includes and extends to the southeast of downtown Los Angeles. We completed installation of three research-grade stationary monitors in the SFV5 study area. We also installed a research-grade monitor at the University of Southern California campus west of downtown Los Angeles. To supplement the data collected from these stationary monitors, we designed and executed

multiple mobile transects. To identify the causative factors of the local heat and cool islands at the neighborhood scale, we collected detailed LULC datasets for the LA Basin, such as 1-m (3.3 ft) resolution roof albedo and tree canopy cover, as inputs for the meteorological modeling and analysis. The fine-scale meteorological model was used to (a) design mobile-transect routes and (b) site the stationary weather monitors based on the definition of UHI / UCI areas.

2: Literature Review

2.1 Modeling the Urban Heat Island Effect

Various approaches have been developed recently to represent the effects of urban areas in atmospheric models. Many of these parameterizations have been implemented in such models as the Town Energy Balance (TEB) of Masson (2000), the microclimate model ENVI_MET (ENVI_MET 2018; Bruse and Fleer 1998), and the urban Weather and Research Forecasting (WRF) Model (Chen et al. 2010).

Three main urban modules are available in the WRF Model. The first approach is based on the urban canopy model of Kusaka et al. (2001), which is a single-layer model representing an urban canyon. The second and third approaches are based on the multi-level urban canopy models Building Environment Parameterization (BEP) and the Building Environment Parameterization–Building Energy Model (BEP-BEM) (Martilli et al. 2002; Chen et al. 2010).

2.2 Measurement of Urban Heat Islands

UHIs can be measured through different methods, including remote sensing, stationary monitors, and mobile measurements. Remotely sensed satellite data can be used to measure surface-temperature UHIs. However, remote sensing is limited to measurement of surface-UHIs because the satellite imagery represents the surface temperature, and the relationship between surface temperature and air temperature is not one-to-one. The difference between surface and air temperatures is influenced by many parameters such as height above ground, solar radiation, wind speed, wind direction, humidity, and surface roughness (Weng 2009). Another limitation to remote sensing is the coarse image resolution (10 – 100 m) which yields homogenous input characteristics for small neighborhoods (Voogt and Oke 1998). Stationary measurements of air temperatures can be used to detect signals in locations across a city, but this type of measurement can be limited by availability of existing research-grade monitors and/or sites willing to host new such monitors. Mobile measurements are easy to tailor and control but provide less temporal coverage than continuously operated stationary monitors.

2.3 Effect of Land Use / Land Cover on Urban Heat Islands

Characterization of urban heat and its causative factors, such as land-surface properties, is an important first step towards designing countermeasures (Taha 2013; Sailor et al. 2016). Relating the urban heat to variations in land-cover and physical properties in urban areas is also critical in understanding how future changes in land use can affect heat islands, and, hence, the efficacy of mitigation measures.

At the fine intra-urban scales—e.g., less than or equal to 1 km (0.62 mi.)—three factors may affect microclimate and heat. These are (1) urban surface albedo; (2) vegetation cover and related shading, soil moisture, and evapotranspiration effects; and (3) urban morphology and related parameters such as sky-view factor and surface roughness (Taha 2008; Jin et al. 2018).

Several studies have used mobile platforms to measure urban microclimate parameters, especially air temperature. For example, Qiu et al. (2017) carried out automobile observations to quantify the effects of green (vegetated) spaces on the UHI in Shenzhen, China. The study focused on ability of evapotranspiration to reduce air temperatures and found that green spaces are the coolest elements of the urban environment, with diurnal-average air temperatures up to ~1.6 °C (2.9 °F) lower than observed for other land uses.

Tsin et al. (2016) compared on-foot mobile transect air temperature measurements in Vancouver, Canada to temperature readings from stationary monitors and to Landsat land-surface temperature. They found that the temperatures measured via transects varied more than those observed at stationary monitoring stations. This was because the mobile measurements were carried out in streets and urban canyons, and thus were more influenced by microclimate anomalies. Jonsson (2004) used mobile measurements to show that the intra-urban variability in air temperature resulting from changes in vegetation cover is of the same magnitude as the urban-rural temperature difference. In this case, evapotranspirative cooling created a summer midday urban oasis of 2 °C (3.6 °F) relative to rural surroundings in Gaborone, Botswana. Herbel et al. (2016) used mobile measurements to measure air temperatures 2 m above ground level (AGL) in Cluj-Napoca, Romania. They found urban areas with high-rise buildings experienced summer evening air temperatures up to 2 °C (3.6 °F) warmer than in surrounding vegetated areas, while air temperatures in low-rise, low-density urban areas were not detectably different from those in vegetated areas.

Some workers—e.g., Sun et al. (2009)—have used mobile observations and stationary monitoring to characterize winter UHIs in Phoenix, AZ. They found that LULC is an important factor in intra-urban UHI magnitude. They also showed that vegetated areas are the coolest regions within the urban areas both day and night.

Ellis et al. (2015) deployed 10 stationary weather stations in different land-use types across Knoxville, TN, for summertime observations of the UHI. The sensors were 2.25 m above ground level. They found that vegetation cover had a significant cooling effect, lowering maximum daytime temperature by up to ~1.2 °C (2.2 °F), but with smaller reductions at night.

3: Methodology

3.1 Acquisition of External Weather Measurements

To help inform placement of our stationary monitors and to provide observations to compare to modeled temperatures, we created a database of accessible historic weather data available for the LA Basin.

3.1.1 Criteria

Observations from different sources can vary in temporal resolution, spatial coverage, spatial density, and accuracy. We created a database of weather observations including all sources that had at least 10 stations available in the LA Basin.

3.1.2 Process

We collected data from existing stationary weather station networks, including the California Irrigation Management Information System (CIMIS), WeatherBug, and Weather Underground (Table 1).

Table 1. Selected weather station networks and their features

Source of data	Number of stations	Temporal coverage	Price
CIMIS	240 in California	2005-2014	Free to public
WeatherBug	424 in Southern California	2005-2015	Free (donated)
Weather Underground	>9000 stations in California	Varies by station	Varies by the type of access

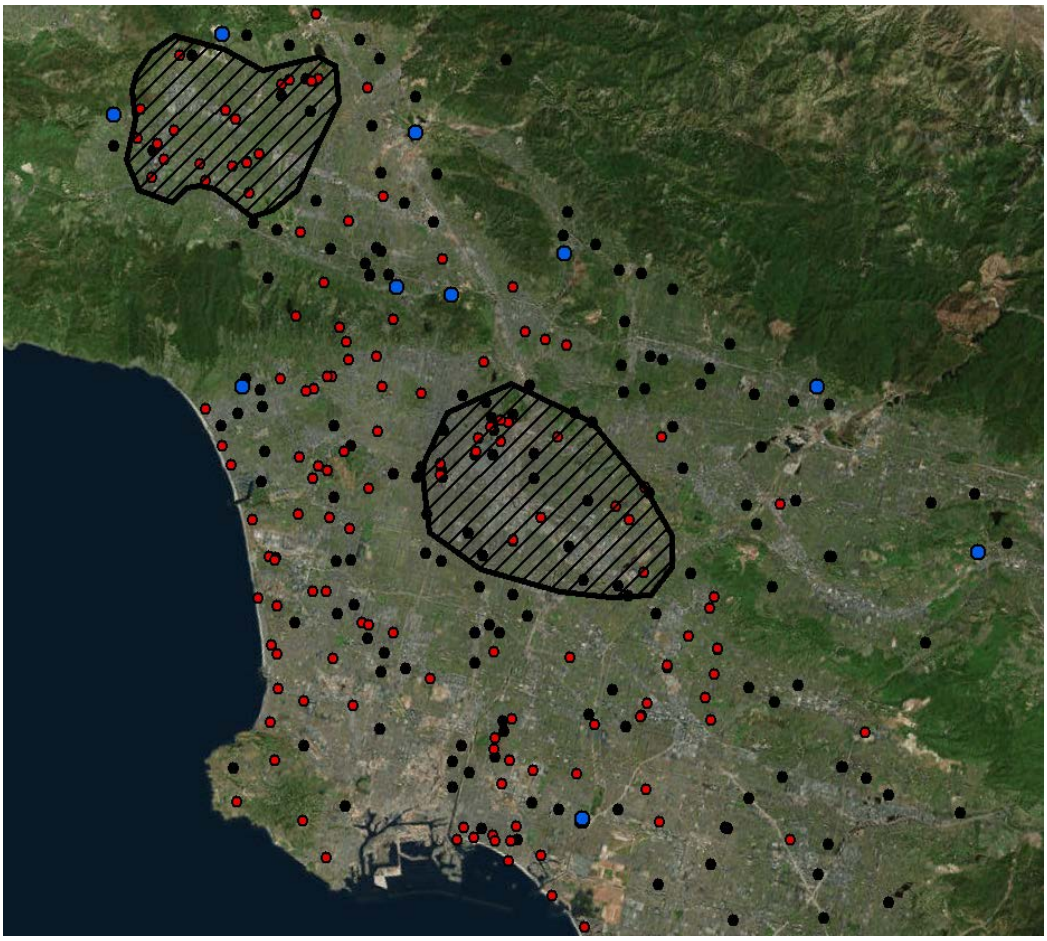

Figure 1 shows a map of all the existing weather stations we included in the database. Data from CIMIS were free, data from WeatherBug were donated, and data from the Weather Underground were purchased. We had limited access to the Weather Underground network API (Weather Underground 2016), so we focused primarily on obtaining data for the areas of interest (presented in Section 0). We also downloaded data from other areas in the LA Basin for possible use in future research studies. Most monitors in the WeatherBug and Weather Underground networks are personal weather stations (PWSes). These networks have higher spatial density (i.e. more stations in the LA basin) compared to many government-operated weather station networks such as CIMIS. While PWSes have better spatial coverage than government stations, the raw data from these networks are not preprocessed. Other drawbacks include (1) PWS equipment is typically less accurate (though also less expensive) than that found in research grade stationary monitors; (2) air temperature sensors in a PWS may be inadequately shielded from the sun; and (3) there are no rules guiding where a PWS may be installed, so measurement variations between stations may result from nearby surrounding objects.

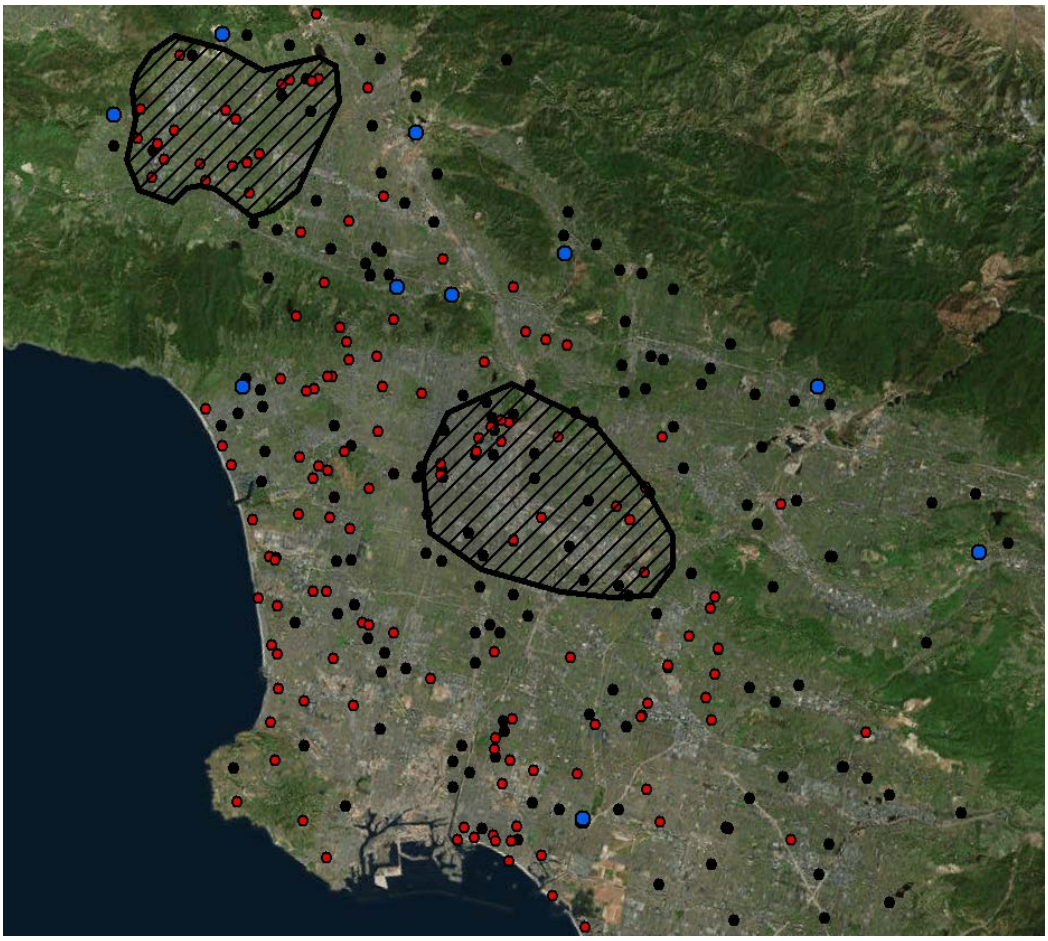

Figure 1. Points on the map locate existing weather stations. The cross-hatched black polygons outline our initial study areas of interest. The red, blue, and black points identify Weather Underground, WeatherBug, and CIMIS weather stations, respectively.

The collected data was stored in a MySQL (open-source relational database management system) database. The database included two sections. The first section details each station, including name, location, elevation, and temporal coverage. The second section lists all the historic meteorological observations collected from all the stations.

3.1.3 Quality Review

Data downloaded from the existing weather station sources was post-processed to remove outliers. This was an important step for the development of the database, since the outliers could make it difficult to detect UHI / UCI.

The cleaning process was completed in three steps. In the first step, we removed null data, which typically represent faulty measurements; these are usually reported as out-of-range values, such as "-999". Unit transformations can make it tricky to identify null values in PWS data. For example, a PWS network that converts ft/s to m/s might transform a null wind speed value of -999 (ft/s) to -304 (m/s). In the second step, we removed the values that were outside the historical range of maximum and minimum observations reported by NOAA weather stations across the LA Basin. In the third step, we removed stations sited in atypical urban settings, such as neighborhoods near golf courses or water reservoirs.

3.1.4 Datasets Selected

We included data from Weather Underground, WeatherBug, and CIMIS in our database of historical observations. Table 1 shows the selected datasets and their features. However, for simplicity and to avoid temperature differences that might result from variations in measurement techniques between networks, our analysis of PWS data only included monitors from the Weather Underground network. The analysis focused on the summer of 2015.

3.2 Study Area Identification

3.2.1 Characterization of Land Use / Land Cover (LULC)

LULC analysis was the first step in identifying urban areas with delineations or transitions of interest—i.e., changes in physical properties. Depending on the region of interest, various sources of LULC information may exist that can be used to characterize the surface properties in a geographical domain. For the LA Basin, these can include: (1) 30-m (98-ft) horizontal resolution National Land Cover Data (NLCD) (MRLC 2014); (2) 30-m horizontal resolution USGS Level-II classification LULC (Anderson et al. 2001); (3) area-specific LULC, such as data developed by the City of Los Angeles; (4) area-specific LULC and building outlines / footprints, such as data developed by the County of Los Angeles (LARIAC 2008); (5) Google Earth morphological and land-cover data for the region; (6) satellite-derived building-specific roof albedo from a Berkeley Lab study of the City of Los Angeles that was performed for the California Air Resource Board (Ban-Weiss et al. 2014); (7) 1-m horizontal resolution area-specific urban morphological and geometrical data from the National Urban Datasets and Portal Tool (NUDAPT) (Burian et al. 2003) for a few areas in the region; (8) fine-scale USGS Level-IV LULC (SCAG 2012) for the County of Los Angeles that include about 100 different classes of land use; and (9) 1-m horizontal resolution EarthDefine / CALFIRE urban tree canopy cover (Bjorkman et al. 2015) for the region.

The study area was then characterized using these data sources. Gridded parameters for surface characterization were developed including albedo; soil moisture; roughness length; drag coefficient; thermal emissivity; plan-, top-, and frontal-area densities for building and vegetation canopy; floor-to-plan ratio; height-to-width ratio; shade factor; sky-view factor; and leaf-area index.

The LULC characterization was performed to (1) derive surface inputs to the meteorological model, and (2) to provide a basis for relating observed air temperature to LULC properties at stationary monitor sites or along mobile-transect routes. Crosswalks (correlations) among the different datasets were also developed so that each grid cell of the modeling domain could be characterized based on several sources of information. Figure 2 and Figure 3 depict examples of LULC characterization in two study areas selected in this project. This was one basis for the initial selection of study areas for further fine-scale modeling and monitoring.

Based on these LULC characterizations, four study areas were identified initially. These are shown in Figure 4. Subsequent fine-scale climate modeling and analysis led to the selection of "LA1" and "SFV5" as the two study areas for conducting the project's mobile transects and detailed meteorological modeling, as discussed in this report. The area identified as "SFV5" in this analysis is actually one of several areas we identified in the San Fernando Valley and "LA1" contains downtown Los Angeles in its northwestern tip. For lack of a better geographical description, LA1 is also referred to as "downtown area" in some of the following sections.

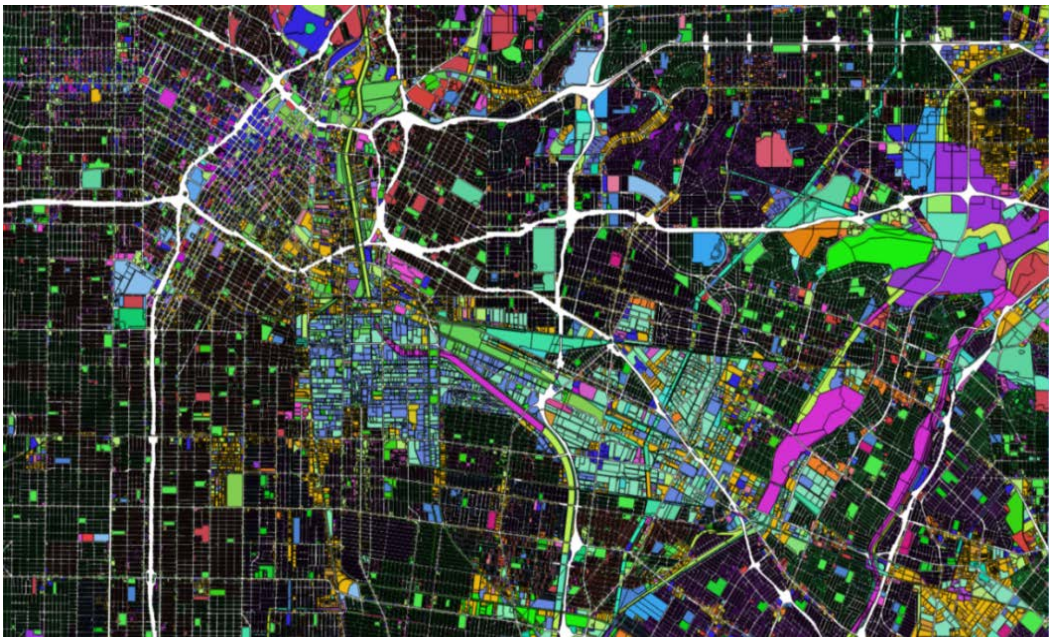

Figure 2. Sample detail from the LULC analysis showing an area including downtown Los Angeles (area LA1). There are about 50 LULC classes represented in this figure; the USGS Level-IV system includes more than 100 classifications. The darker areas are residential land uses and the ones color-coded blue, dark green, and red in the middle are industrial and commercial land functions. Bright green represents open and/or vegetated areas (Data source: SCAG 2012).

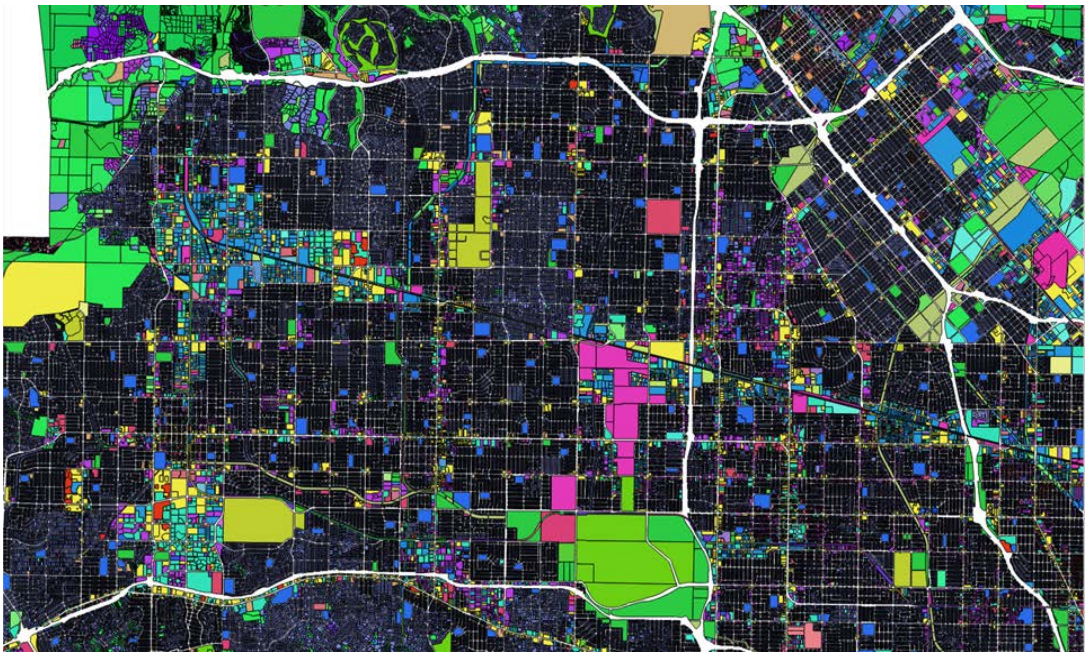

Figure 3. Sample detail from LULC analysis showing the San Fernando Valley and area SFV5 in the upper-left part of the figure, selected for modeling and observational analysis. The darker areas are residential land uses and the ones color-coded blue, dark green, red, and yellow are industrial, commercial, and academic land functions. Bright green are open and/or vegetated areas. Magenta is transportation (in this case, Van Nuys airport). (Data source: SCAG 2012)

Figure 4. Boundaries of initial study areas LA1, LA2, LA3, and SFV5 (solid white lines) considered for meteorological modeling, installation of new stationary monitors, and mobile transects; LA1 and SFV5 were selected. Also shown are the boundaries of study areas Central LA and SFV_R (solid gold lines) used in analysis of personal weather station data, and the boundaries of the San Fernando Valley (SFV) and Downtown LA (dotted white lines).

The grid-cell-level albedo is computed by accounting for LULC components including (1) roofs, (2) pavements, (3) vegetation, (4) water surfaces, and (5) other cell-specific land functions that were derived from the LULC data sources discussed above.

Roof albedo is computed based on remote-sensed values from LBNL dataset (Ban-Weiss et al. 2014) and is thus highly building- and cell-specific. Pavement albedo is computed based on past research of California (Akbari et al. 1999; Rose et al. 2003) and the USGS Level-II classifications system (Taha 2007). Vegetation and water were assigned constant values of albedo based on field measurements and literature review (Taha et al. 2015).

Tree canopy cover characterization was based on 1-m horizontal resolution data from Earth Define / CALFIRE (Bjorkman et al. 2015). The 1-m data is binary – each pixel is set to 1 if a tree canopy is present, or to 0 otherwise. This was then up-scaled to 500 m (1640 ft) resolution. While the EarthDefine / CALFIRE data are categorized into low, medium, and high tree-canopy cover, this study calculates tree-canopy cover with a range from 0 – 100% based on the up-scaling of the pixel values.

Characterization of cell-specific building geometrical / morphological parameters in this study (e.g., plan- frontal-, and top-area densities; mean height; and sky-view factor) relies primarily

on calculations performed using detailed buildings footprints and geometry information, and secondarily on NUDAPT and prior Google Earth Pro analysis of Californian urban areas (Taha 2008a-c).

To compute the building-specific site area, the calculations subtract vegetation cover and building plan area from the total cell area, then divide the remainder by the number of buildings to determine an average open-space area per building that is then used to compute the building plan-area density. In the vertical direction, calculations were repeated at 5-m (16.4-ft) intervals to compute the percentage of total building plan area (in a grid cell) that exists within each specified height interval.

The vegetation roughness length parameter and building roughness length parameter were characterized for each grid cell based on the approach of MacDonald et al. (1998). To calculate roughness length in this manner, several morphological variables were derived for every grid cell as discussed above. These include (1) frontal area densities of roughness elements (buildings and vegetation), (2) plan-area densities, and (3) heights. In addition, empirical coefficients and correction factors were assigned per Macdonald et al. (1998) and Grimmond and Oke (1999).

3.2.2 Climate Modeling Results and Suggestions for Study Areas

The detailed meteorological modeling performed in this study helped us site stationary weather monitors and plan mobile-monitoring routes. The modeling results also provided a basis for correlating micrometeorology at each site with the surrounding LULC characteristics affecting temperature, i.e., local heat or cool islands (UHI or UCI).

The Weather Research and Forecasting – Advanced Research WRF (WRF-ARW) meteorological modeling system (Skamarock et al. 2008) was selected for use in this study. Several urban parameterizations were applied and inter-compared. Meteorological input for the summers of 2013 and 2006 was prepared as in a prior modeling effort for a Cal/EPA project (Taha and Freed 2015). These periods represent typical summer and heat-wave conditions in California and are used in this project for the sake of compatibility with the Cal/EPA California Urban Heat Island Index (UHII) modeling work (Taha 2017). The UHII was developed in response to California AB 296 to characterize both the extent and severity of the urban heat island effect in California's cities.

The two study areas identified (LA1 and SFV5) were modeled to assess the potential UHI and/or UCI signals that stationary monitors and mobile transects in this area would capture. The meteorological modeling domain was configured such that the finest grids (500-m resolution) encompass these two areas of interest.

Four periods were first simulated to evaluate whether the near-surface air temperature field and UHI and/or UCI patterns are significantly altered in different summer conditions. These periods are (1) May 30 through June 16, 2013, representing relatively typical summer conditions in California; (2) June 29 through July 16, 2013, representing warmer conditions; (3) June 30 through July 16, 2006, representing windier conditions; and (4) July 14 through August 1, 2006, representing the California heat wave of 2006 (Gershunov et al. 2009).

The simulations were done with model customizations that begin by overriding default, lookup-value model input with domain-specific surface characterizations that are defined for each grid cell in a bottom-up approach (Taha 2017). This approach improves the area-specificity

of surface inputs to the meteorological model, including surface albedo, vegetation cover, roughness length, soil moisture, shade factor, and other parameters discussed above. This was then refined in the study by modifying the urban canopy model of Kusaka et al. (2001) as discussed in Taha (2017).

The simulated temperature field was then characterized for each grid point in the modeling domain using two diagnostics. The first diagnostic is 2-m (6.6-ft) air temperature (T_{air}) calculated from interpolation between surface and first atmospheric level. The second diagnostic is 2-m air temperature based on surface temperature and heat transfer calculations, typically referred to as "T2" in the modeling environment. Thus, T_{air} is more representative of the prognostic (predicted) temperature field within and above the urban canopy layer (UCL), including advective effects, whereas T2 is more of a diagnostic air temperature that is representative of localized in-UCL air temperatures.

Based on results from this analysis, several points in the LA1 and SFV5 domains were identified as localized UHI or UCI areas; examples are shown in Figure 6 and Figure 7. The modeled temperature was converted into degree-hour (DH) metrics to capture cumulative rather than instantaneous properties of the temperature field. (Degree-hours are computed as the time integral of temperature). The goal was to evaluate whether the general temperature pattern was consistent across the different summer conditions considered in this study. The spatial pattern of the temperature field was found to be similar (repeatable) for intervals modeled in this study. Therefore, the spatial characteristics can be used as basis for development of siting criteria.

Additional details on the approach used in the current study can be found in Taha et al. (2018).

3.2.3 Preliminary Mobile Transects to Select Areas

To quantitatively evaluate the model prediction of temperature tendency and spatial gradients in temperature in the modeled areas, preliminary mobile-transect measurements of temperature were devised for initial feedback and preparation for more rigorous model performance evaluation. The transect was conducted in LA1 during April 2016. The observations confirmed the findings from the model, allowing us to use the modeled results to identify the study areas of interest. These aspects are discussed in detail in the project report (Levinson et al. 2018).

3.2.4 Study Areas Selected

Based on the initial results discussed in Section 3.2.2, we decided to install monitors in the San Fernando Valley area SFV5 and in area LA1 to capture the interactions between LULC and microclimates in (1) inland regions (the San Fernando Valley) and (2) areas influenced by the sea breeze flow and climate archipelago effects (the semi-coastal region that includes area LA1). (An archipelago is group of islands, or a body of water containing a group of islands; we use the term "climate archipelago" to refer to the complex climate effects of a very large, continuous urban area since upwind portions can affect downwind portions.) Monitoring two different areas can help us understand the role of local surface-properties and impacts on temperature in different climate regimes—here, inland valleys and quasi-coastal areas.

3.2.4.1 Criteria

The horizontal (geographical) siting of monitors depends on LULC analysis and meteorological-modeling results as discussed in Section 3.2.2. Choosing the height at which to install stationary monitors relies on flow theory, as discussed below. However, there are non-technical limitations on siting, including availability, site accessibility, and jurisdiction by project partners

in the region. In some cases, the final selection of monitor sites could be decided solely by these non-technical limitations.

To understand spatial variations in UHI and their interactions with land-use and land-cover properties, and to develop mitigation measures, the scale of interest is about 500 m – 1500 m (0.3 mi – 0.9 mi).

Thus, an appropriate height needs to be determined for placing monitors above the ground surface or above roof level to capture land-cover effects within an upwind distance of 500 m – 1500 m. Ideally, air temperature sensors should be sufficiently removed from ground, wall, or roof surfaces to avoid measuring a temperature that is affected directly and solely by these surfaces (grey bar in Figure 5), but not so high above ground or roof surfaces such that the temperature readings become regional in nature and unrelated to the 500 m – 1500 m fetch of interest. Thus, it is desirable to place the sensors vertically within the range indicated with the blue bar in Figure 5. Flow theory can provide some general guidance in this respect (Cheng and Castro 2002; Arya 1988; Panofsky and Dutton 1984).

A transition in roughness or surface properties, in this case a change in LULC physical properties, induces an internal boundary layer (IBL) that grows downwind of the transition area. In this project, it is desirable to place the sensors within the internal boundary layer corresponding to the land-cover being characterized. If the sensors are placed above the IBL, then the temperature readings will be those of the background flow, unrelated to the fetch (LULC) of interest. Based on approximations by WMO (2006), and assuming a blending height (Z_r) (see Figure 5) that is 1.2 - 1.5 times the building height (in dense and/or homogeneous urban areas), the calculations suggest that placing the sensors at a height of ~2 m above ground surface or above roof level would be suitable for the length scales of interest in this study.

Several monitors installed during this project, as well as existing network monitors in the region, are all at ~ 2 m above roof level, which corresponds to the elevation at or slightly above the blending height shown in the figure. This is the desirable height for measuring the surface effects over a 0.5 – 1 km upwind fetch. For the same reason, mobile-transect measurements were carried out at 2 m above ground level to capture effects of surroundings at that scale. It is possible to relate the mobile measurements to fixed, above-roof measurements by taking the average of many mobile observations that correspond to the area “seen” by the fixed monitors.

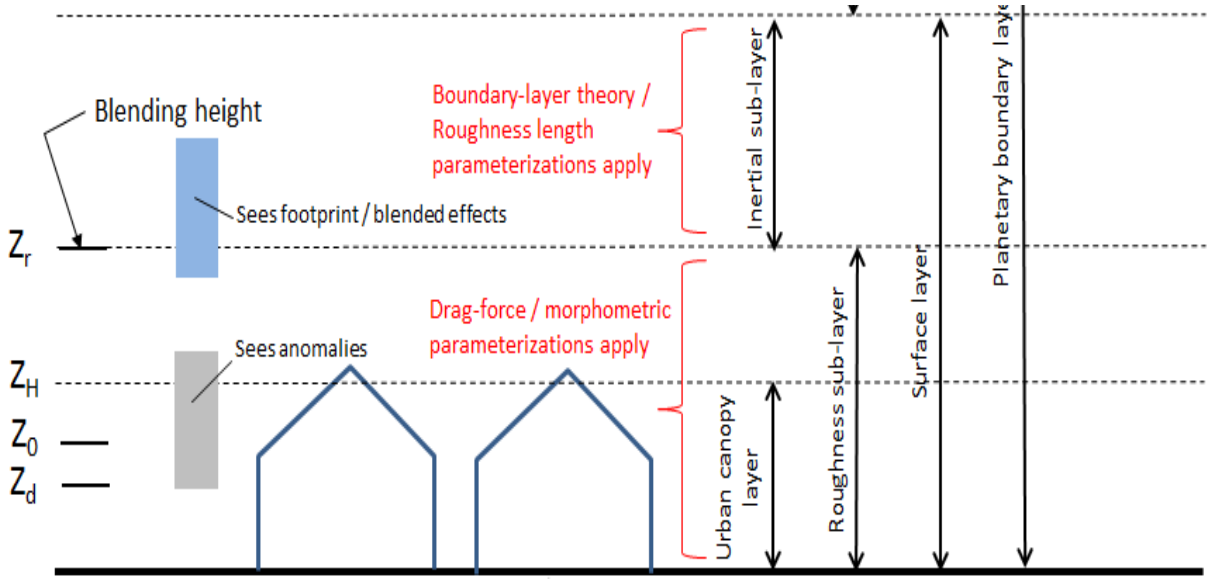

Figure 5. Parameter definitions in relation to vertical placement of weather monitors (temperature, wind direction and speed, and solar radiation). Figure is not to scale. The urban canopy layer is defined as a layer below roof level; the roughness sub-layer is in the order of 1.5 times the roof height; and the planetary boundary layer is on order of hundreds of meters at night and up to several kilometers during the day.

3.2.4.2 Coordination with project partners

Several points in the LA1 and SFV5 study areas were identified as localized UHI or UCI areas based on model and initial mobile-transect results. We shared these points and study areas with project partners—including the City of Los Angeles, County of Los Angeles, and LAUSD—and collectively developed a list of their facilities that could serve as potential sites for the stationary monitors.

3.2.4.3 Identification of potential sites for stationary monitors

The suggested sites were evaluated based on technical criteria and location relative to model-predicted UHI / UCI points. A summary listing and evaluation of all potential sites (30 possible locations) is provided in the project report (Levinson et al. 2018). Upon further evaluation of these sites via examination of three-dimensional imagery (e.g., Google Earth Pro) and location visits, certain sites were assigned a lower priority because of such factors as (1) unavailability of flat roofs (sloped roofs can be an issue for installing weather stations), (2) lack of secure sites in open areas (at ground level), and (3) physical characteristics of the site. This resulted in a top tier of ten potential sites. Some of these sites in LA1 and SFV5 are shown in Figure 6 and Figure 7.

While we developed a list of the top ten potential sites, we struggled to get local approval and find suitable locations at each of the sites for the installation of the monitors. We had high-level support from our partners. However, many layers of approval were required, especially as we honed in on specific sites and locations. For instance, we had support from City of LA Fire Department management to install monitors, but we ran into a barrier with the labor union representing the firefighters, which did not want a rooftop monitor on their fire station transmitting data via a cellular modem.

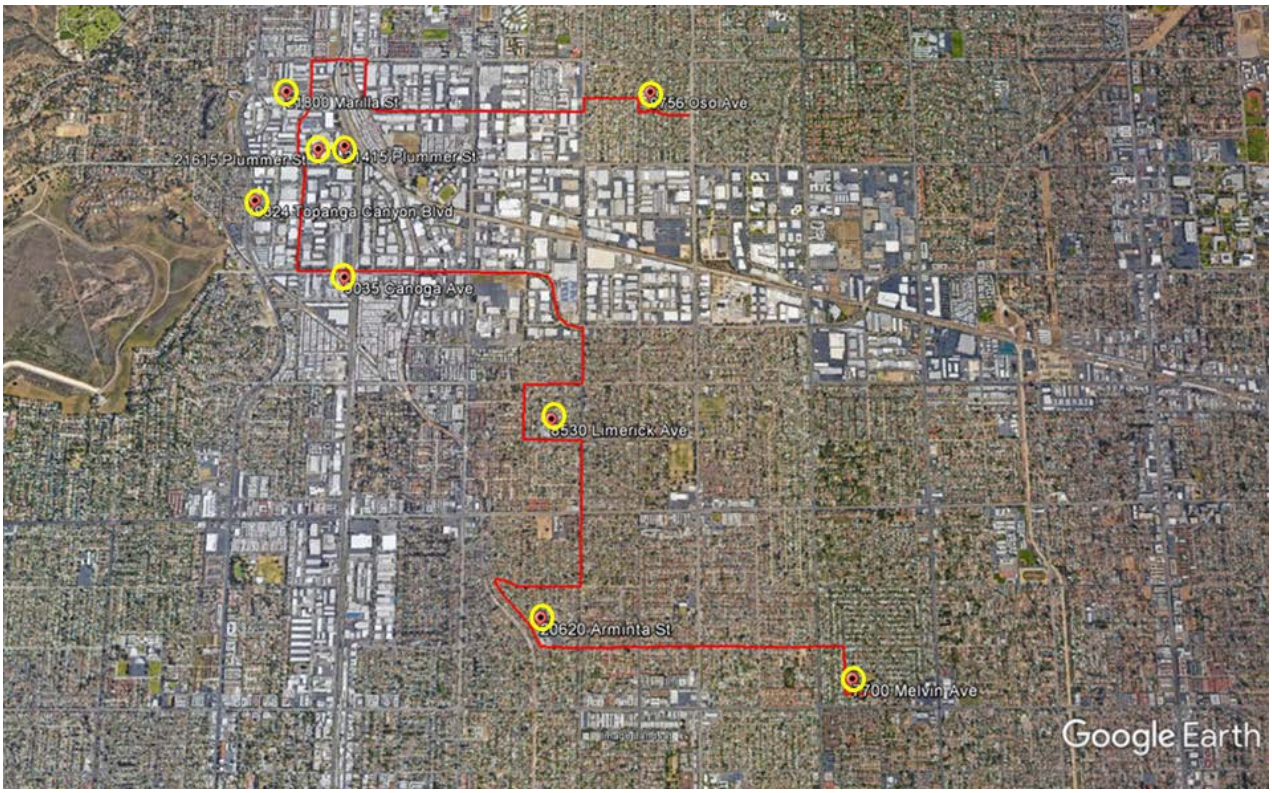

Figure 6. Prospective monitoring sites selected in the San Fernando Valley (red markers circled in yellow) with a sample mobile-transect route.

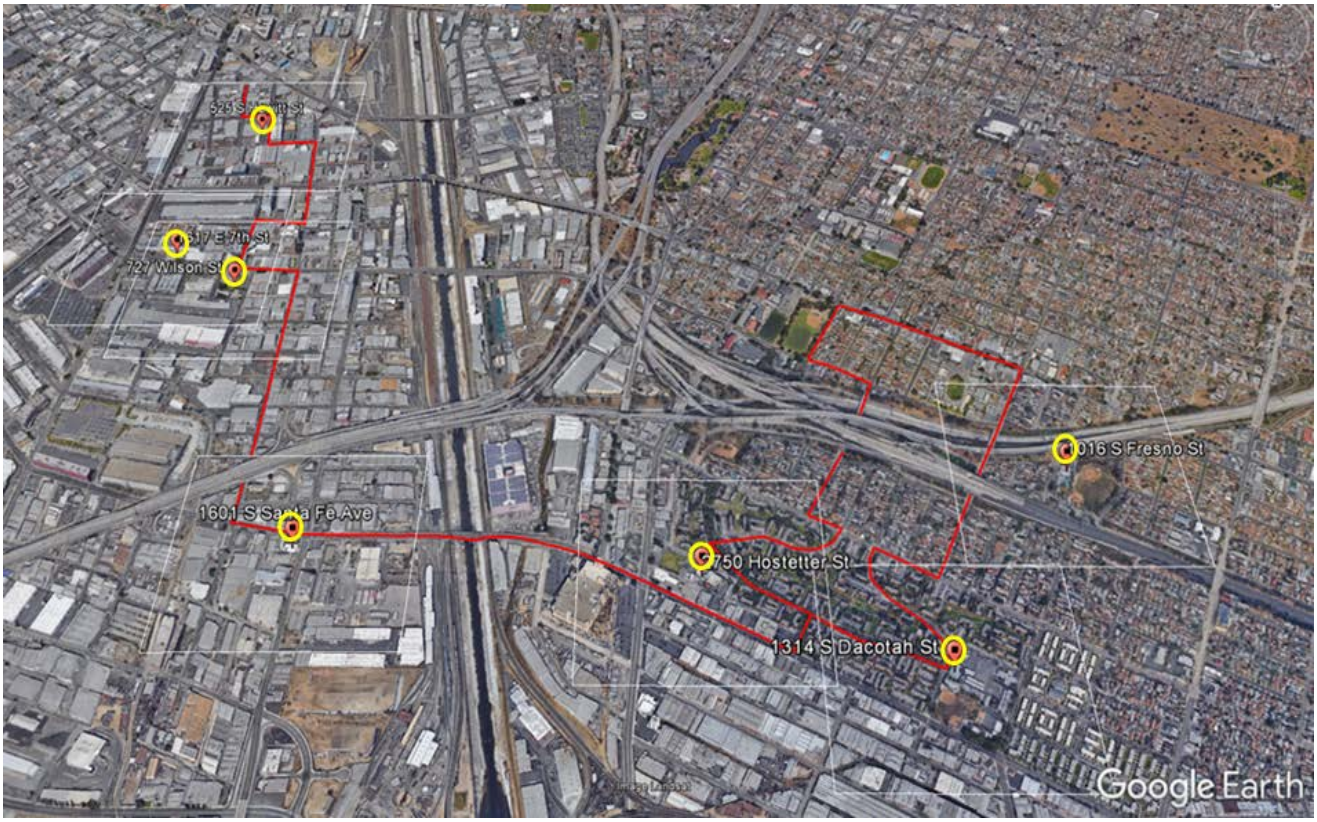

Figure 7. Monitoring sites (red markers circled in yellow) selected in the downtown Los Angeles area (LA1) with a sample mobile-transect route.

3.3 Stationary Weather Measurement

3.3.1 Criteria

We desired the following characteristics for each monitor.

1. The monitor should accurately and continuously measure the primary signal, dry-bulb air temperature; secondary signals, including wind speed, wind direction, solar irradiance, and relative humidity, useful for interpreting variations in air temperature; and monitor diagnostics, such as radiation-shield fan speed, needed to verify that the sensors are operating as designed.
2. To facilitate initial installation and subsequent maintenance, the monitor should be easy to assemble and program.
3. The monitor should be readily installed on an elevated surface, such as that of a low-slope roof, to measure air temperature at some fixed height above ground.
4. The monitor should communicate over the internet or by cellular modem for convenient data collection and (if necessary) reprogramming.
5. The monitor should be durable, ideally with a service life approaching a decade.

The monitor should cost less than $5K, in accordance with our proposed budget.

3.3.2 Monitor Design

A **monitor** typically comprises multiple weather sensors, a logger, and a support structure. The monitor will run off a battery charged by local AC power or a photovoltaic (PV) panel. If the monitor is to be accessed remotely, it will also have an internet connection, landline modem, or cellular modem.

Dry-bulb air temperature can be measured with several types of sensors, including but not limited to thermistor (ceramic resistance thermometer), resistance temperature detector (RTD; metal resistance thermometer), or thermocouple. Sensor choice depends on measurement range, speed, and accuracy, as well as instrument cost and durability. While each technology has merit, a precision thermistor is a low-cost, high accuracy option with sufficient range.

When air temperature is measured outdoors, the sensor should be **shielded and aspirated** (ventilated) to reduce errors induced by short-wave (solar) and long-wave (thermal infrared) radiation. This can be accomplished by installing the sensor in a commercial or custom aspirated radiation shield. A commercial unit will typically output a signal indicating its fan speed, which can be monitored to verify that the sensor is being aspirated.

Wind speed can be measured with several types of sensor, including but not limited to three-cup anemometer, vane anemometer, hot-wire anemometer, ultrasonic anemometer, or pressure anemometer. Wind direction is usually measured with a wind vane. Weather stations will usually employ a three-cup anemometer to measure speed and a wind vane to measure direction, or a vane anemometer that determines both speed and direction.

Downwelling solar irradiance can be measured with a thermopile pyranometer or a semiconductor pyranometer. If solar irradiance is a secondary parameter, a less expensive semiconductor pyranometer will suffice. Note that if one needs to measure upwelling sunlight—say, to determine solar reflectance of a ground or roof surface—downwelling and upwelling solar radiation should each be measured with a thermopile pyranometer.

Relative humidity (RH) can be measured with several types of sensor, including but not limited to resistive hygrometer or capacitive hygrometer. A resistive hygrometer bases its RH determination on both the resistance and temperature of a sensing element, and therefore is integrated into a device that reports both RH and temperature.

A **logger** (also known as a data logger) typically integrates a programmable microprocessor, analog/digital inputs, analog/digital outputs, non-volatile memory, telecommunication hardware, and battery into a standalone unit that operates the sensors, locally stores their output, and may intermittently transmit recorded measurements to a remote computer or cloud data server.

We reviewed the specifications and prices of two loggers, six wind speed/direction sensor kits, two silicon pyranometers, two temperature sensors, one RH sensor, and four aspirated radiation shields. We also factored in our positive and negative experiences with some of these instruments in past projects.

After considering all these inputs, we specified and purchased a system from Onset Corporation that connects to a logger (RX3000) plug-and-play digital-output sensors that measure wind speed (S-WSB-M003 three-cup anenometer), wind direction (S-WDA-M003 wind vane), solar irradiance (LIB-M003 silicon pyranometer), and temperature/RH (S-THB-M002 temperature/RH). The logger also has a four-channel analog module (RXMOD-A1) that can excite and measure analog signals, such as the output of a thermistor circuit (air temperature) and a pulse-counting circuit (fan speed). The logger can upload its measurements to a cloud data server via cellular modem. All components can be mounted on a tripod structure, which in turn can be installed on a roof.

Relevant specifications of the Onset sensors and logger are summarized by Levinson et al. (2018).

We acquired evaluation units of two aspirated radiation shields—the RM Young (RMY) 43502, and the Apogee Instruments (AI) TS-100 (Table 6)—and an Onset U23 Pro v2 external temperature/relative humidity (T/RH) data logger (U23-002), which is a standalone version of the T/RH smart sensor (THB-M002) used in the monitor. We also purchased two models of precision thermistors: the US Sensor KS103G2, and the Apogee Instruments ST-110.

Following extensive testing (Levinson et al. 2018), we determined that the AI and RMY shields were each suitable for our purpose. We selected the AI shield because (a) it draws much less power, which may prove helpful if a monitor's battery must be charged with a PV panel; and (b) it is easier to mount a thermistor (though not a T/RH sensor) in the center of the air flow. While we were impressed with the high accuracy and low cost of the KS103G2 thermistor, it does not include the cabling or the voltage divider circuit needed to use it as a temperature sensor. Since our experience is that is more economical to buy a complete product than to purchase and assemble components, we selected the AI ST-110 thermistor, which is more expensive but is ready to connect to the logger's analog input module.

3.3.3 Monitor Calibration

We had final partner approvals to install four monitors. The four monitors were calibrated at the University of Southern California (USC) before three of them were installed at the selected locations. During a four-day period (July 21, 2017 - July 24, 2017), the four monitors were installed at a USC campus parking lot. Monitor_0 was the reference station installed at USC (see Section 0 for more details). Measurements from the other monitors were compared to this reference monitor. During this calibration period, we moved the monitors around the site and switched the location of the sensors and other equipment on the monitor (e.g., fans) that could affect our measurements. We did this to investigate and compare the potential biases caused by station location and sensor placement. Negligible differences were observed from the slight differences of location of monitors (e.g. distance from near objects, containers). The overall results of the calibration did not show any significant difference between the sensors from the different monitors.

3.3.4 Stationary Monitor Installation

Four stationary monitors (Monitor_0 - Monitor_3) were installed between Oct 2016 to Apr 2018. We installed three in SFV5, and one near the USC campus, which served as the reference monitor (Monitor_0) (Figure 8). The process of negotiation to find sites, suitable locations at sites, and acquiring the needed approvals to host the monitors took much longer than expected. The first monitor (Monitor_0) was installed on USC's campus inside a gated area in a parking lot. This location was easily accessible for the research team, and thus served as the permanent location for our reference monitor (Monitor_0) and the location for calibrating the other monitors. Monitor_0 was installed on October 26, 2016. The sensors were installed 2 m above ground level and the monitor was stabilized with ballasts. Monitor_1 was installed at the City of Los Angeles' Bureau of Street Services Facility Yard in Topanga Canyon on July 25, 2017. The monitor was installed 2 m above the roof surface on a structure that provides shade to a parking lot. It was also secured with ballasts. Monitor_2 was installed at LAUSD's Sunny Brae Elementary School on January 11, 2018. The monitor was installed on the roof 2 m above the roof surface on a school building and secured to an existing pole. Monitor_3 was installed at LAUSD's Melvin Elementary School on April 13, 2018. The monitor was installed 2 m above the roof surface on a school building and secured to an existing roof antenna pole. For both Monitor_2 and Monitor_3, staff from LAUSD assisted with the installation to guarantee that safety procedures were followed.

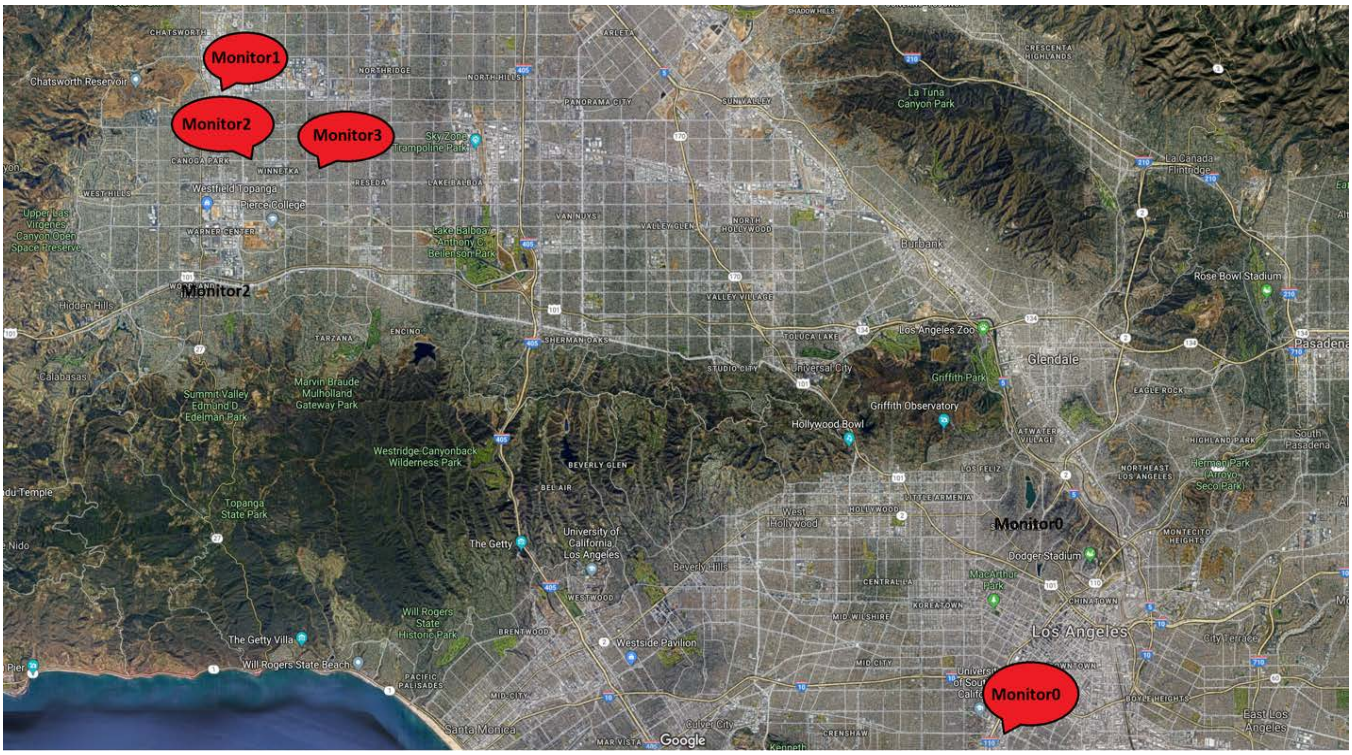

Figure 8. Location of the four installed monitors on the map on Los Angeles.

3.3.5 Monitor Operation

Data collection began as soon as each monitor was installed. The observations are collected at 10-second intervals, and the average for each minute is recorded. The data is transmitted from each monitor to the service provider (HOBOLink) using a cellular modem; we can access the data, visualize, export, and order frequent delivery via email to our servers or accounts. We also have set up a publicly available feed on the Weather Underground website from our monitors installed on schools, since the LAUSD and the schools themselves were interested in exploring the gathered data.

Unfortunately, the selection and negotiation for the locations of the monitors took longer than predicted; by the time we installed the last station (April 13, 2018), we were getting to the end of the project. Thus, we could not incorporate them in the analysis presented here. The data will be available for future projects and analyses.

3.4 Mobile Observation Path Selection

Mobile-observation transects were carried out to measure microclimate variations along the routes. Of particular interest is air temperature variation, as the LULC and surface properties change along each route segment. The goal was to develop correlations that quantify the responses in temperature to changes in albedo and vegetation canopy.

Points of interest (e.g., UHI and UCI) were identified in both the SFV5 and LA1 domains based on their modeled temperature-field characteristics.

The selected mobile-observation routes were designed such that they cut across the LULC boundaries and transitions, e.g., to capture the possible effects of changes in LULC from one

neighborhood to another. The routes also were designed to yield small changes in elevation and to keep the duration of each transect sub-segment under 20 minutes (to minimize variations in air temperature that result from change in time of day).

In all, 15 transects were carried out in summers of 2016 and 2017 in both SFV5 and LA1 (as will be discussed in Sections 3.7 and 4.2.2). Figure 9 shows a composite of all transects that were carried out, as well as a random example detail of one transect sub-segment. Some transect routes are duplicates (superimposed on each other) and hence appear as one. While all transects shown in LA1 were considered in the analysis, only the parts of the transects within the red box were considered in the analysis for SFV5.

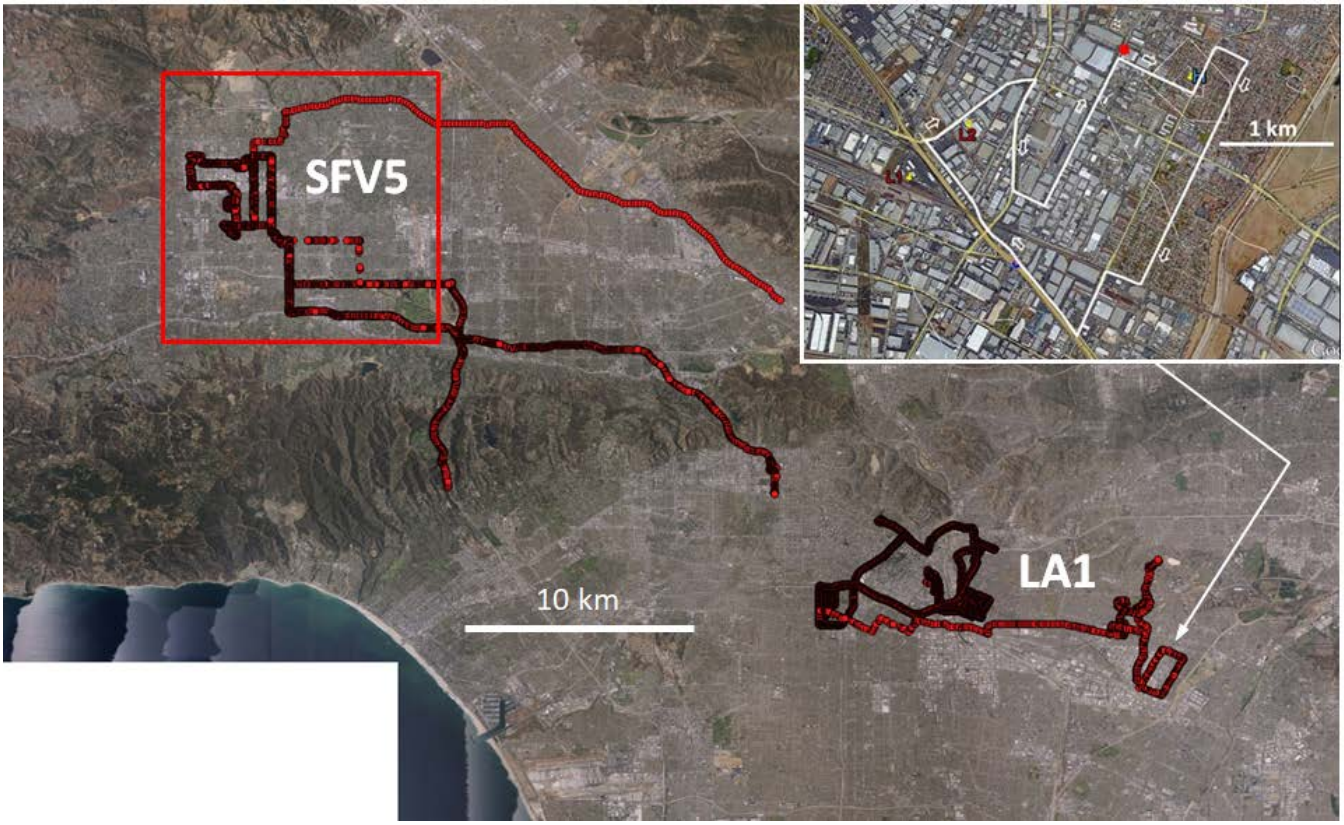

Figure 9. Superimposed routes of 15 transects. While all transects shown in area "LA1" were considered in the analysis, only the parts of the transects within the red box were considered in the analysis for SFV5. Inset: example detail.

3.5 Mobile Monitor Design and Operation

3.5.1 Design

Horizontal variations in air temperature near the ground (say, 2 m above ground level) can be mapped by attaching a thermometer to roof of a vehicle, such as a car, then logging temperature, position, and time during a transect. To ensure that the thermometer accurately measures air temperature, its sensor should be aspirated by the motion of the vehicle, shielded from the sun, and radiatively isolated from its shield. The sensor should also respond quickly to

air temperature changes to minimize spatial inaccuracies, or blurring, in the air temperature map induced by the motion of the vehicle.

Our mobile transect apparatus (hereafter, the apparatus) contains five elements: (1) a shielded temperature sensor aspirated by vehicle motion; (2) a quick-install mount to attach the shielded sensor to the roof of a vehicle; (3) a portable data logger to record the temperature time series; (4) a global positioning system (GPS) to record the position time series; and (5) a dash camera (dash-cam) to record time-stamped video of the transect from the perspective of the driver.

Shielded temperature sensor. To minimize sensor response time and blurring of the temperature map, we selected a small negative temperature coefficient thermistor (US Sensor model KS103G2, diameter 2.5 mm (0.098 in), electrical resistance 10 kΩ @ 25 °C [77 °F]; US$5) shown in Figure 10 as the temperature sensor. The manufacturer-reported time constant of this bead thermistor is not more than 10 s in still air, and should be substantially less in moving air. Note that a 5 s delay in response will yield a 50 m (164 ft) error in temperature measurement location if the apparatus is traveling at 10 m/s (22 mph). Since, in the analysis, air temperature at each observation point along the transect was related to surface properties within radii of influence of 500 m to 1 km, the potential implication of this error is insignificant.

The nominal accuracy of this thermistor is ±0.1 °C [0.18 °F] from 0 to 70 °C [32 to 158 °F], with an operating range of -80 to 135 °C [-112 to 275 °F].

To minimize the sensor's solar heat gain, we installed it at the center of a 25" length of size 6, schedule 40 white PVC pipe (length 63.5 cm, outer diameter 16.8 cm, inner diameter 15.4-cm, wall thickness 0.71 cm), as shown in Figure 10. If the pipe is horizontal and faces the sun, it shields the sensor from all beam sunlight when the solar elevation angle is 14° or greater.

We selected a wide pipe to facilitate air flow through the pipe and around the sensor when the length of the shield is parallel to the motion of the vehicle. This enhances convective heat transfer between air and sensor. We estimate that the convective heat transfer coefficient of the sensor is about 80 $W/m^2 \cdot K$ at an air speed of 1 m/s (2.2 mph), rising to 170 $W/m^2 \cdot K$ at 5 m/s (11 mph), 240 $W/m^2 \cdot K$ at 10 m/s (22 mph), and 340 $W/m^2 \cdot K$ at 20 m/s (45 mph).

To minimize radiative heat transfer between the sensor and the inner surface of the shield, we wrapped the sensor in aluminum foil. (Since the sensor is essentially enclosed by the much larger shield, there is little benefit to foil-lining the inner surface of the shield, which will act as a black body cavity regardless of its thermal emittance.) The foil has an initial (clean) thermal emittance of about 0.03. If soiling by dust in the air increases the foil's thermal emittance to 0.10, the radiative heat transfer coefficient between the foil-wrapped sensor and the shield will be about 0.6 $W/m^2 \cdot K$. This is about 400 times smaller than the convective heat transfer coefficient when the sensor is in a 10 m/s air stream. Note that even if the foil were to vanish, the radiative heat transfer coefficient from the bare sensor (thermal emittance about 0.90) to the shield would be about 5.5 $W/m^2 \cdot K$. This remains about 40 times smaller than the sensor's convective heat transfer coefficient in a 10 m/s (22 mph) air stream.

Quick-install mount. We built a quick-install mount for the shielded sensor that places the bead about 48 cm [19 in] above the roof of the vehicle, or about 2 m (6.6 ft) above ground level when installed on 1.5 m [4.9 ft] tall passenger car. Vertical risers support the shield over pair of removable aluminum mounting bars (Proline Racks model CB-602 universal roof rack; US$40) with straps that hook to the vehicle's frame, while crossbeams horizontally stabilize the

mounting bars. The risers, crossbeams, and assorted fittings are all made of PVC. Each mounting bar rests on wide plastic feet with rubber soles that protect the roof (Figure 11).

The shield is permanently affixed to the mount, but the mount itself can be attached to a vehicle roof (Figure 11) in about 10 minutes.

Portable data logger. A handheld, battery-powered data logger with LCD screen (Lascar Electronics model EL-USB-TP-LCD; US$100) records temperatures measured with the thermistor. The logger can store a time-stamped series of up to 32,000 values with a resolution of 0.1 °C [0.18 °F] and a frequency of up to 1 measurement per second. We detached the thermistor probe supplied with the data logger because the probe encapsulates its thermistor in a 75 mm long, stainless steel tube expected to respond slowly to changes in air temperature (Figure 12). We substituted the US Sensor bead thermistor described above, which was chosen to match exactly the resistance versus temperature curve of the thermistor in the original probe. The bead thermistor was soldered to the end of a 4 m [13 ft] cable that plugs into the logger, which in turn is placed inside the car. The cable is snaked through a slightly open window.

Temperature measurements are recorded at 1 Hz, at which frequency the logger can store nearly 9 hours of data. The logger must communicate with a computer to start logging and to download results, but can record data by itself, and does not require external power. The logger's clock is set to network time when connected to the computer.

Global positioning system. A smartphone app (MapMyTracks, iOS/Android; free) uses GPS and/or cellular tower data to record a time-stamped series of locations (latitude, longitude) at a frequency of one measurement every two to three seconds. The location time series is stored in the cloud, and later downloaded. The phone must be externally powered while recording position to avoid draining its battery.

Note that while both the smartphone clock and the temperature logger clock are synced to network time, the logger records temperatures more frequently than the location app records positions. Therefore, the combination of logger and app yields spatially located temperature measurements at the frequency of the location app (~ 0.3 to 0.5 Hz).

Dashboard camera. A dashboard camera (KDLINKS model X1; US$170) records high-definition, time-stamped video through the vehicle's windshield, storing up to 88 min of 1920 by 1280 pixel, 30 frame/sec imagery on a 32 GB memory card (generic; US$15). The camera must be externally powered while recording video to avoid draining its battery.

The camera is manually synced to network time to ensure that the times and dates displayed on the video match those recorded by the temperature logger and location app. While the use of a camera is optional, it provides a visual record of the transect for later reference.

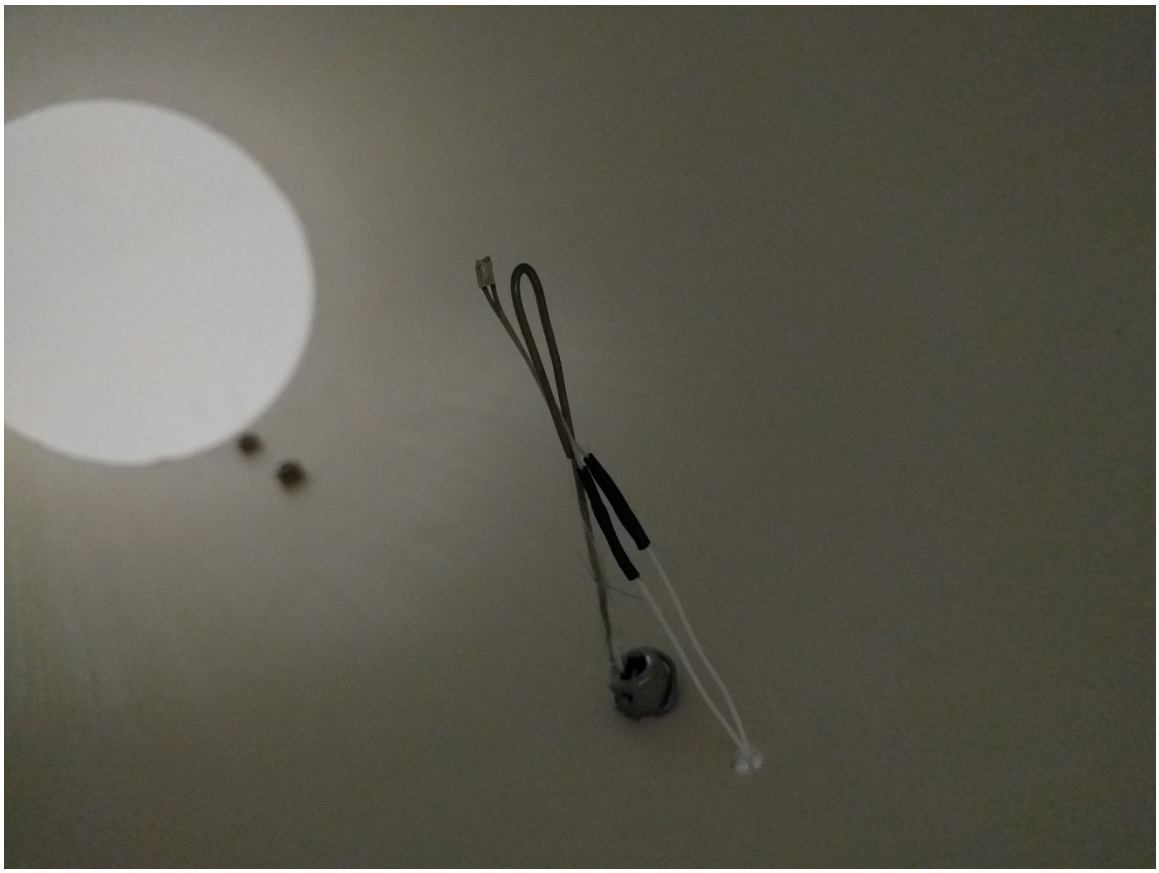

Figure 10. Bead thermistor wrapped in aluminum foil, then secured with clip in center of shield.

Figure 11. Shield on quick-install mount, strapped to the roof of a car, including white PVC-pipe shield, gray PVC-pipe vertical risers, aluminum tube roof mounting on plastic and rubber feet, and white PVC-pipe crossbeams. Straps with hooks (not shown) secure the bars to the vehicle frame.

Figure 12. Temperature logger shown with stock thermistor probe. The detachable probe was replaced by a 4 m extension cable leading to the foil-wrapped bead thermistor shown in Figure 10.

3.5.2 Calibration

We did not calibrate the temperature sensor to an ice bath or other reference because (a) its function is to map variations in air temperature, rather than absolute air temperature; (b) the nominal accuracy of the sensor is high (±0.1 °C from 0 to 70 °C); and (c) the major potential source of error is radiative heating via absorption of sunlight or exchange of long-wave radiation with the shield (pipe). As noted in Section 0, we took three steps to minimize such error. First, if the pipe is horizontal and faces the sun, it shields the sensor from all beam sunlight when the solar elevation angle is 14° or greater. Hence, the sensor will never be in direct sun unless the apparatus is used near sunrise or sunset. Second, we wrapped the sensor in aluminum foil, making the coefficient for long-wave radiative heat transfer between wrapped sensor and pipe 400 times smaller than that for convective heat transfer between the wrapped sensor and a 10 m/s air stream. Third, even if the foil were to come off, the coefficient for long-wave radiative heat transfer between bare sensor and pipe would still be 40 times smaller than that for convective heat transfer between the bare sensor and 10 m/s air stream.

3.5.3 Operation

We completed fifteen transects in total during 2016 and 2017 in the two study areas—SFV5 and LA1. Figure 9 shows the transect routes in the two study areas. Table 2 details the date, time, and the study area of each transect.

The first transects were conducted in personal vehicles, with two researchers in each vehicle—one to drive, and the other to make measurements. We soon switched to ride-sharing services, hiring Uber drivers to install the apparatus on their car and drive along our transect paths with a researcher in the car to manage the equipment. This proved to be a time- and cost-efficient improvement because (1) it was cheaper to hire Uber than to reimburse researchers for personal vehicle use and (2) only one researcher was needed in the car.

The design of the apparatus also withstood the wear and tear from being installed, uninstalled, and stored over the project duration. Hurdles to carrying out the mobile transects included time wasted being stuck in traffic traveling to and from study areas, the need to modify initial transect routes on the fly because of unexpected road construction and closures, and crime safety concerns (that went unmerited) of driving through certain locations at night (20:00-22:00 LDT1).

3.6 Calibration of climate model to observations

For the summer periods (May, June, July, and August) in years 2006 - 2013, the model produces generally similar (repeatable) spatial patterns of air temperature in each region and relatively consistent geographical locations of UHI and UCI. Figure 13 and Figure 14 depict the modeled 2-m air temperature field (shown as degree-hours) for May 30 - June 16 (2013) in the two 500-m domains containing LA1 and SFV5. The purpose of the top graph in each figure is to give an idea where certain temperature patterns occur relative to the urban and geographical features in the area, and how the model captures the cooling and heating effects of certain land covers such as parks, large roof areas, and roadways. In the bottom graphs, the corresponding domains are shown again but without the background, for easier visualization and assessment of the

1 Los Angeles is in the Pacific time zone, where local daylight time is UTC/GMT -7 hours.

temperature field characteristics. The contours are color-coded ranging from low to high degree-hours (blue to red); the figure captions provide additional information.

In LA1 (Figure 13), the modeled air-temperature field captures the on-shore warming tendency and also the consistently warmer commercial and industrial areas southeast of the Arts District, including the cities of Vernon, Maywood, and Commerce. In the northeastern parts of this domain, the model shows warmer urban areas in the region between the cities of Monterey Park and Alhambra and also between Lincoln Heights and South Glendale. The temperature field also captures many areas of localized cool islands, mostly associated with open and/or green spaces and some areas with higher urban albedo. It can be seen in Figure 13 that the effects of on-shore warming are significant and that the localized UHI / UCI effects are superimposed on this signal (Taha 2017).

In the San Fernando Valley domain (Figure 14), sea-breeze effects are negligible and temperature is influenced mainly by topography and variations in land use and surface properties. The model predicts higher temperatures in the industrial and commercial areas from near Chatsworth in the north, to Canoga Park, and Woodland Hills in the south. Higher model temperatures are also seen along the major roadways, including, for example, Sherman Way and Parthenia Street (running west to east) and Reseda Boulevard (running north to south), among others. Cool islands in this domain are associated with areas of higher vegetation cover.

The temperature field in these figures clarifies the locations of the localized heat and cool islands in the area.

Model performance evaluation was carried out against fine-scale observations from mobile transects. For transect-specific modeling (500-m resolution), modeled air temperature was compared to observations from transects at the coincident time (sub-hourly intervals). The goal was to ascertain successful model capture of the micrometeorological variations in the urban areas and to validate the modified WRF model against the mobile observations. Both modeled and observed air temperatures from mobile transects were assessed at 2 m AGL.

While the transect-specific WRF model (TSM) runs were initiated a week ahead of the actual transect time and were continued for 2 days past that, performance evaluation for TSM runs was carried out only and specifically at the transect time. The statistics reported in Table 2 compare along-transect observations with along-transect WRF-model temperature and demonstrate a very satisfactory performance for the approach adopted in this study. Table 2 reports both mean absolute error (MAE) and root mean square error (RSME) in temperature. Both the MAE and RMSE in temperature are significantly better than the recommended performance benchmarks of MAE ≤ 2°C [3.6 °F] and RMSE ≤ 2°C [3.6 °F] (Tesche et al. 2001). The results in the table demonstrate good agreement between along-transect roadway observations and area-averaged model results.

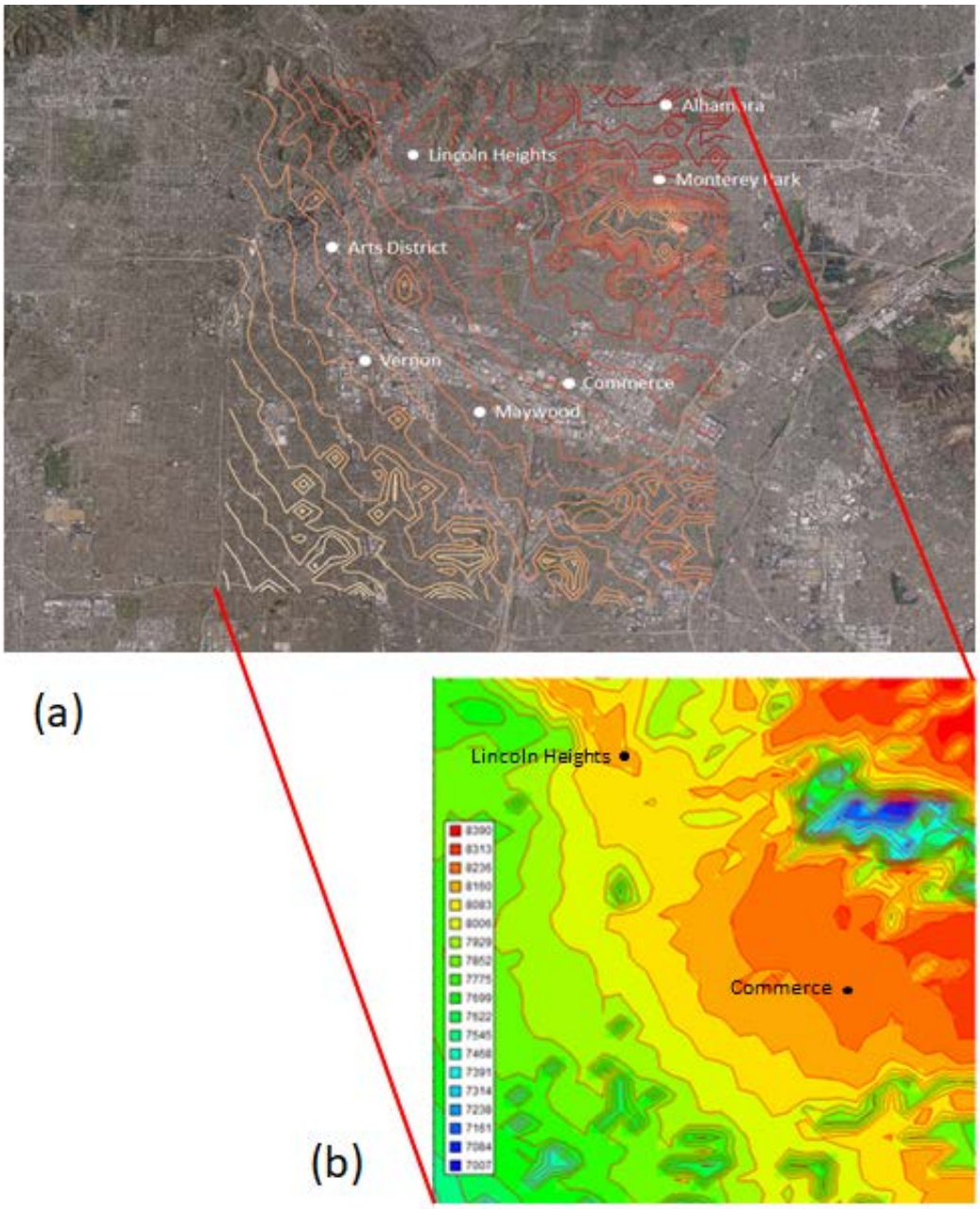

Figure 13. Total degree-hours (DH) for interval May 30 – June 16 (2013) in downtown LA 500-m domain (LA1). The derived average temperature (computed as DH/hour), blue to red, is 17.2–20.6 °C (62.9 – 69.1 °F) for this period. Color bar is total DH, range: 7,007 – 8,390.

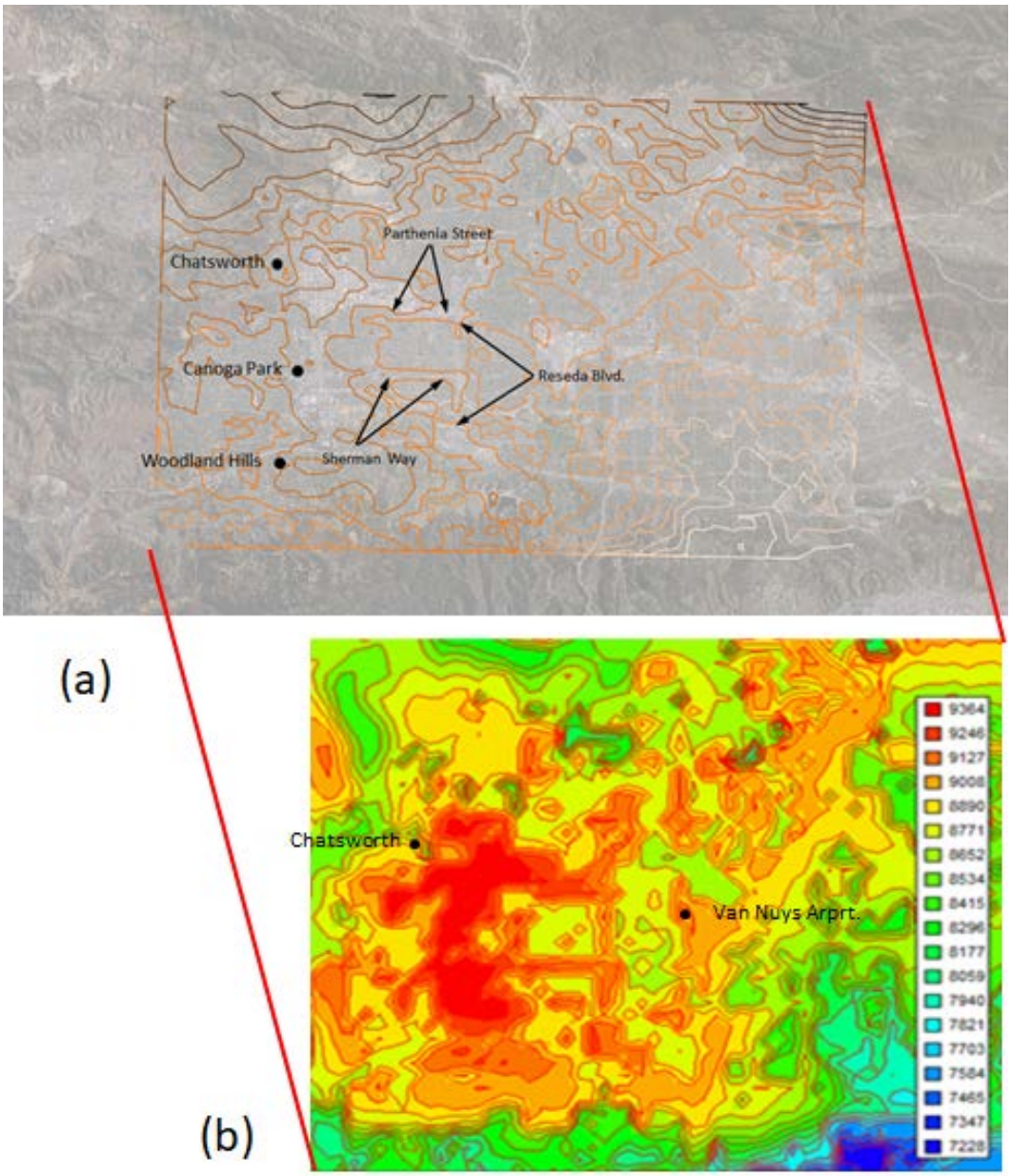

Figure 14. Total degree-hours (DH) for interval May 30 – June 16 (2013) in the San Fernando Valley 500-m domain (SFV5 is in the western part of this domain). The derived average temperature (computed as DH/hour), blue to red, is 17.7–22.9 °C (63.9 – 73.2 °F) for this period. Color bar is total DH, range: 7,228 – 9,364.

Table 2. Model performance metrics against observational mobile-transect temperature. The date, time, and location (either SFV5 or LA1) of each transect is listed. Note that transect TR14 is omitted from this analysis because of missing data.

TRANSECT	Mean Absolute Error in Temperature (°C) [°F]	Root Mean Square Error in Temperature (°C) [°F]
2016_04_22 (LA1)	1.15 [2.07]	1.33 [2.39]
2017_06_14 Part 1 (LA1)	0.88 [1.58]	1.00 [1.80]
2017_06_14 Part 2 (LA1)	0.61 [1.09]	0.76 [1.36]
2017_06_14 Part 3 (LA1)	0.80 [1.44]	0.94 [1.69]
2017_06_14 Part 4 (LA1)	0.70 [1.26]	0.86 [1.54]
2017_06_21 (SFV5)	1.73 [3.11]	2.00 [3.60]
2017_07_27 day Part 1 (SFV5)	0.97 [1.74]	1.20 [2.16]
2017_07_27 day Part 2 (SFV5)	0.92 [1.66]	1.10 [1.98]
2017_07_27 night Part 1 (SFV5)	0.55 [0.99]	0.68 [1.22]
2017_07_27 night Part 2 (SFV5)	0.85 [1.53]	1.00 [1.80]
2017_08_28 day Part 1 (LA1)	0.48 [0.86]	0.60 [1.08]
2017_08_28 day Part 2 (LA1)	0.71 [1.27]	0.94 [1.69]
2017_08_28 night Part 1 (LA1)	1.00 [1.80]	1.10 [1.98]
2017_08_28 night Part 2 (LA1)	0.82 [1.47]	0.92 [1.65]

3.6.1 Description and Data Sources for Land Use Land Cover Properties Used in Personal Weather Station Analysis

For the analysis of personal weather stations, we have chosen two study areas ("regions") of interest within the Los Angeles Basin. Each region was chosen to fulfill two requirements: (1) it should be sufficiently small such that distance from the coast does not dominate temperature variations; and (2) there should be sufficient variation in land cover properties of interest (e.g.,

roof albedo) to enable discerning effects of land cover on measured air temperatures. The first region encompasses an area of roughly 500 km^2 and includes downtown Los Angeles; we refer to this region as Central Los Angeles. (Note that Central Los Angeles contains all of LA1.) The second region encompasses roughly 160 km^2 and is located within the San Fernando Valley; we refer to this region as SFV_R.

We used somewhat different datasets describing land use land cover properties (referred to as "LULC" from this point on) for the analysis of personal weather stations. LULC properties were computed using data from multiple sources for each neighborhood as described below.

Roof fraction (f_{roof}) represents the ratio of building roof area (i.e., assumed to be equivalent to building footprint area) to neighborhood area. Roof fraction is computed using the Los Angeles Region Imagery Acquisition Consortium (LARIAC) dataset shapefiles for building footprints (LARIAC 2008).

Tree fraction (f_{tree}) is computed using a tree dataset from LARIAC with spatial resolution of 4 feet (1.2 m). This dataset is binary, indicating whether or not each pixel has tree cover. Analogous to roof fraction, the tree fraction represents the ratio of tree covered area to neighborhood area.

Pavement fraction (f_{pavement}) represents the area fraction of pavements per neighborhood, with pavement area contributions from parking lots and paved road. Parking lot area is computed using parking lot boundaries given by LARIAC dataset shapefiles. Paved road area is derived using a street centerline dataset (CAMS 2011). The total road length is computed by summing roadway length per neighborhood, and road area is then calculated by multiplying by an assumed road width of 12.8 m. Note that this road width represents the average street plus sidewalk width for Los Angeles, calculated using the weighted mean road width per building type (CARB 2017), where the weighting factor is determined using the relative quantify of different building types in LA.

Reflected solar power from roofs (P_{roof}) represents the average daily solar power (W) reflected from roofs within the neighborhood. This is computed as

$$P_{\text{roof}} = I \times \alpha_{\text{roof}} \times f_{\text{roof}} \times A \qquad (1)$$

*w*here I is the average daily incoming solar power (W m^{-2}), α_{roof} is the weighted average roof albedo in the neighborhood, and A is the neighborhood area ($\pi \times 500$ m^2 = 7.85×10^5 m^2) (see the next section for more information on the neighborhood areas). The average daily solar power of the day includes all 24 hours, not just sunlit hours. The area-weighted mean roof albedo (α_{roof}) is determined using a dataset for seven California cities that reports building-specific roof albedos using remote sensing data (Ban-Weiss et al. 2015); the mean roof albedo is computed for each neighborhood using the roof's area as the weighting factor. Overall, the metric P_{roof} is used to account for the influence of cool roofs, considering (a) the mean roof albedo of the neighborhood, (b) the spatial coverage of roofs in the neighborhood, and (c) the daily solar irradiance. This avoids biases that could occur when, for example, the mean roof albedo of a neighborhood may be high, but spatial coverage of roofs is low.

Reflected solar power from neighborhood ($P_{\text{neighborhood}}$) represents the average daily solar power (W) reflected from the entire neighborhood. This parameter is estimated as

$$P_{\text{neighborhood}} = I \times \alpha_{\text{neighborhood}} \times A \quad (2)$$

where $\alpha_{\text{neighborhood}}$ is the average albedo of the neighborhood. The average neighborhood albedo is estimated using Eq. (3), assuming that the neighborhood is comprised of roofs, pavements, and trees:

$$\alpha_{\text{neighborhood}} = \frac{\alpha_{\text{roof}} * f_{\text{roof}} + \alpha_{\text{pavement}} * f_{\text{pavement}} + \alpha_{\text{tree}} * f_{\text{tree}}}{f_{\text{roof}} + f_{\text{tree}} + f_{\text{pavement}}} \quad (3)$$

Since spatial datasets describing pavement and tree albedos do not exist, we assume values of 0.10 and 0.15, respectively. Due to potential inaccuracies in the GIS datasets, and because neighborhoods can consist of surface types other than roofs, pavements, and trees, $f_{\text{roof}} + f_{\text{tree}} + f_{\text{pavement}}$ generally does not equal 100%. Thus, the denominator of Eq. (3) ensures that neighborhood-to-neighborhood variability in $f_{\text{roof}} + f_{\text{tree}} + f_{\text{pavement}}$ does not lead to variability in neighborhood albedo. While this calculation provides a relatively crude estimate of reflected solar power from the neighborhood, it is sufficient for the purposes of our study since this metric is used only for supporting analysis.

Reflected solar power from non-roof surfaces ($P_{\text{non-roof}}$) represents the average daily solar power (W) reflected from surfaces other than roofs in the neighborhood. This parameter is computed as $P_{\text{neighborhood}}$ minus P_{roof}.

4: Results and Discussion

4.1 Stationary Temperature Measurements

4.1.1 Deriving Sensitivities of Measured Air Temperature to LULC Properties

We compute sensitivity as the linear regression of temperature to LULC properties within a region (i.e. SFV_R or Central Los Angeles) for each hour of every day during July 2015. Thus, each regression looks at temperature versus land cover variability from station to station within a given region. After a multi-step outlier removal process, the sensitivity of temperature to the LULC property is calculated. We perform these regressions for each hour of the day and thus acquire hourly sensitivities for the entire month of July 2015. Investigating sensitivities for each hour of the day can help hypothesize physical processes that are driving the observed correlations. We only compute these regressions for sunny days, defined as those with daily maximum solar irradiance > 700 W m^{-2}.

To ensure that regression results are not dominated by a small number of weather stations, we take the following steps to remove outlier data points:

1. We first detect and remove outlier weather stations for each hour. This is carried out by first performing a standard least squares regression. The influence of each point in determining the regression slope is then computed using leverage and residuals. Based on the distribution of influences for each hour and region, data points that have influence that is beyond 1.5 times the inner quartile range are removed. This effectively removes points that have too much influence in determining the final regression statistics. After these points are removed, another regression is carried out. This time, we use a robust regression with a Huber-T objective function [Huber, 1981]. Regression using the Huber objective function gives higher weights to points with lower residuals, whereas standard regression using least-squares gives equal weights to each observation. The combination of outlier removal and robust regression minimizes the role of observations with both high leverage and residual. We estimate the sensitivity of temperature to the LULC parameter as the slope of the final regression.
2. Next, we determine whether the computed spatial sensitivity is statistically distinguishable from zero. We do so by computing the probability ("p") value of the aforementioned robust regression. We deem the hourly sensitivity significant if the p-value is less than 0.1.
3. Lastly, for each hour of the day, we compute the number of days in July with statistically distinguishable sensitivities for each land cover attribute. Those with more than 10 such days are deemed as having significant relationships for that hour of day. Those with 10 or fewer such days are deemed insignificant.

4.1.2 Spatial and Temporal Profiles

While some of the Weather Underground stations dated back to 2005, we selected year 2015 when there were more station observations to analyze across the LA Basin. Again, we focused on summer months to investigate urban air temperatures during the warm months.

Figure 15 shows the highest summer temperature in 2015 from selected stations across the LA Basin. Figure 16 shows the diurnal range of temperature measurements across LA for different stations during summer after outlier removal.

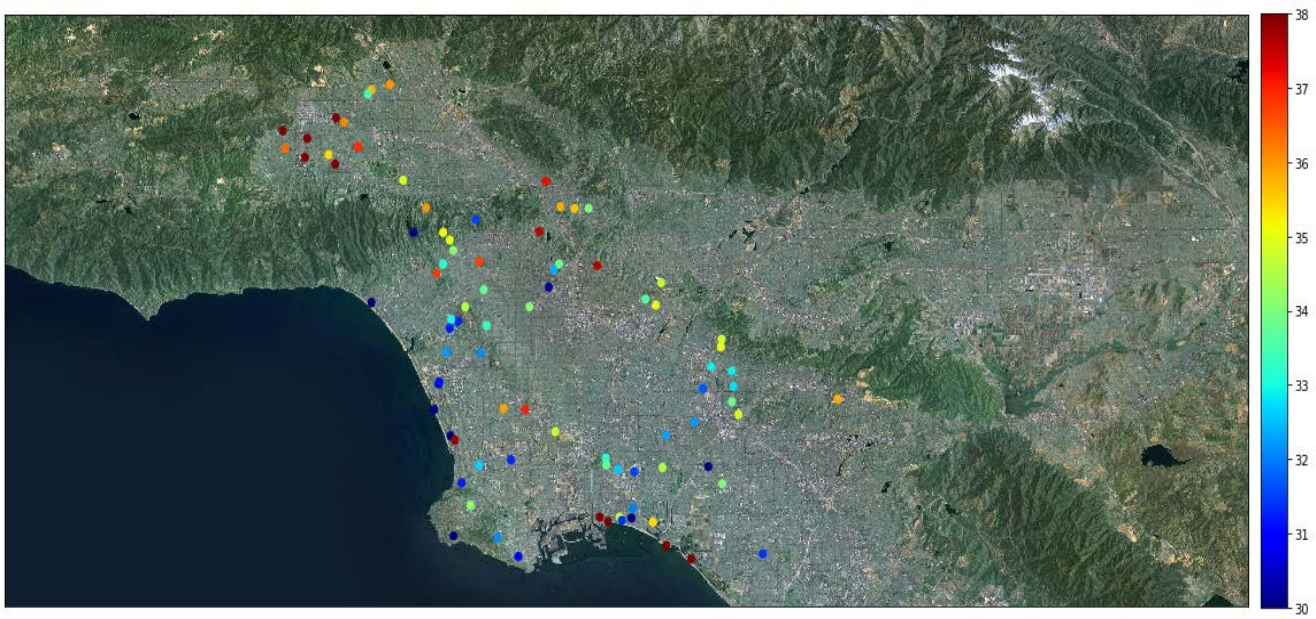

Figure 15. Spatial distribution of Weather Underground stations used in the analysis. Colors indicate each station's peak summer 2015 temperature (°C).

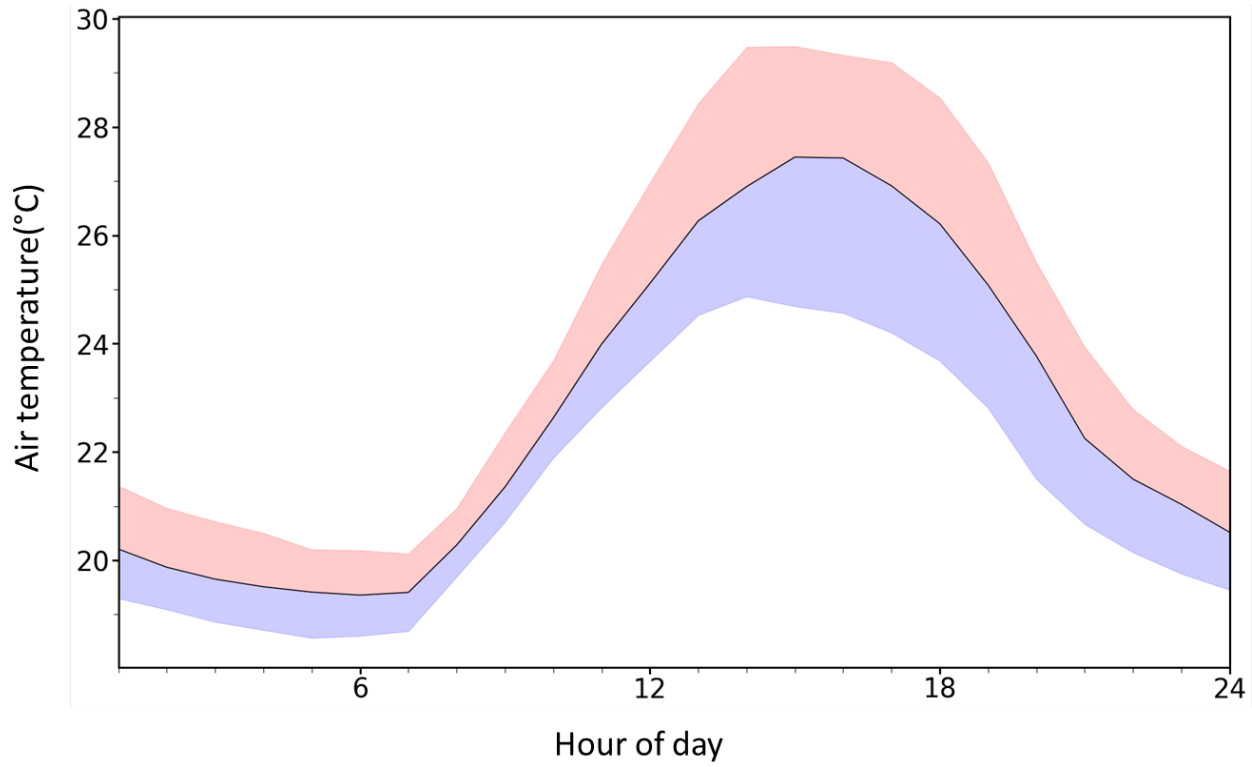

Figure 16. Diurnal range of measured hourly averaged temperature for different stations across the basin. The black line represents the median station, the red range shows the values for stations above the median, and the blue color shows the values for stations below the median, after outlier stations were removed.

4.1.3 Relation to LULC

4.1.3.1 Sensitivity of temperature to solar power reflected from roofs

Panels a and b in Figure 17 present sensitivities of temperature to daily average solar power reflected by roofs for Central Los Angeles and SFV_R, respectively. (Note that sensitivities for the early morning hours, i.e., between midnight and sunrise, use the average solar power of the previous day in calculating the sensitivities, since the previous day's solar power is more relevant in determining temperature of the neighborhood than the average solar power of the upcoming day.) Each box and whisker plot shows the distribution of values for sensitivity per hour over all sunny days (daily maximum solar irradiance > 700 W m^{-2}) in July 2015.

Median hourly sensitivities for Central Los Angeles (Figure 17a) are negative throughout the day, and most of these sensitivities are statistically significant. The largest negative sensitivity occurs at 15:00 LDT, which is roughly consistent with the hottest time of day (i.e., 14:00 LDT in this domain). This matches our expectation based on the underlying physical processes involved since cooling occurs via increased reflected solar radiation. While reflected solar radiation peaks at 13:00 LDT, there is an apparent lag between maximum cooling and maximum radiation. As the sun goes down in the evening, sensitivities trend toward zero, and reach the lowest (negative) sensitivity right before sun rise. This again matches our expectation based on physical mechanisms since the apparent temperature reductions induced by reflected solar radiation from roofs are expected to diminish after the sun goes down. The observed lag between peak temperature reduction and peak solar irradiance, and the non-zero sensitivities at night, are likely caused by thermal inertia of roofs. Note that in Los Angeles, the peak temperature occurs earlier (15:00 LDT) than in many other cities that do not experience an afternoon sea breeze.

Sensitivities of temperature to daily average solar power reflected by roofs for SFV_R (Figure 17b) show a similar diurnal shape as that of Central Los Angeles. However, most hours of the day have sensitivity values that are not statistically significant in SFV_R. Sensitivities at 14:00 and 15:00 LDT are significant, however. While sensitivities for some hours of night are positive, indicating counterintuitively that temperatures are positively correlated with increased daily reflected solar power, these values are not statistically significant.

4.1.3.2 Sensitivity of temperature to tree fraction

Figure 17c and d present sensitivities of temperature to tree fraction for Central Los Angeles and SFV_R, respectively.

In Central Los Angeles, these sensitivities are positive for most sunlit hours of the day and negative at night. The maximum positive sensitivity is observed in the early afternoon (14:00 LDT). The apparent positive sensitivities during daytime are counter to expectation based on the underlying physical mechanisms since increased tree cover should be associated with temperature reductions through increased evaporative cooling and shading of surfaces.

We suggest that these positive daytime sensitivities are actually driven by co-variations between temperature, tree fraction, and daily average reflected power from roofs. To investigate this hypothesis, we present daily average solar power reflected from roofs versus tree fraction for each neighborhood (Figure 18). Solar power reflected from roofs is anti-correlated

(correlation with negative slope) to tree fraction with a coefficient of determination of 0.36. This is consistent with our assertion that solar power reflected from roofs is driving temperature reductions (and apparent positive sensitivities between temperature and tree fraction) since (1) neighborhoods with lower tree fraction are associated with higher solar power reflected from roofs and lower temperatures; and (2) the underlying physical mechanisms suggest that increases in solar power reflected from roofs should lead to temperature reductions, while increases in tree fraction should not lead to temperature increases.

Additional evidence for this assertion is that the diurnal cycles for sensitivity of temperature to (1) daily average solar power reflected from roofs (Figure 17a) versus (2) tree fraction (Figure 17d), nearly mirror each other. The largest negative and positive sensitivity values occur in the early afternoon in panels a and b of Figure 17, respectively. To summarize, we assert that daily average solar power reflected from roofs is likely driving both observed temperature reductions and the apparent positive association between tree fraction and temperature in this region.

For SFV_R, sensitivities of temperature to tree fraction are mostly statistically insignificant, though some values are significant during nighttime. These significant nighttime values are negative, suggesting that increased tree fraction is associated with temperature reductions, as expected based on the underlying physical mechanisms. We do not observe significant positive sensitivity during the day in SFV_R as was observed for Central Los Angeles. We suggest that this is because less of the variance in solar power reflected by roofs is explained through variations in tree fraction in SFV_R ($R^2 = 0.09$) relative to Central Los Angeles ($R^2 = 0.36$). The reduced coefficient of determination (R^2) would lead to less co-variation among temperature, solar power reflected from roofs, and tree fraction.

We note that the sensitivities reported above are likely specific to the region under investigation. Other regions with different baseline (a) tree coverage, (b) tree physical properties, (c) soil moisture, and (d) meteorology, among others, are likely to show different relationships between air temperature and tree fraction.

4.1.3.3 Roof versus non-roof surfaces as contributors to variability in solar power reflected from neighborhoods

In this section we aim to rule out the possibility that apparent temperature reductions associated with increases in solar power reflected by roofs are driven by co-variations in solar power reflected by non-roof surfaces (e.g., vegetation and pavements). To do so, we first present daily average solar power reflected from roofs versus solar power reflected from the neighborhood (Figure 19a). In this analysis, each point represents a different neighborhood. High values of coefficient of determination ($R^2 = 0.80$ for SFV_R and 0.65 for Central Los Angeles) indicate that a large proportion of the variance in solar power reflected from the neighborhood is explainable through variations in solar power reflected from roofs. In Figure 19b, we present daily average reflected solar power from non-roof surfaces versus reflected solar power reflected from the neighborhood. In this case, coefficients of determination are much lower ($R^2 = 0.07$ and 0.10 for SFV_R and Central Los Angeles, respectively). This suggests that variations in daily average solar power reflected from the neighborhood are dominated by variations in solar power reflected by roofs rather than non-roof surfaces. This provides additional evidence that observed temperature reductions are being driven by increases in solar power reflected by roofs in these regions.

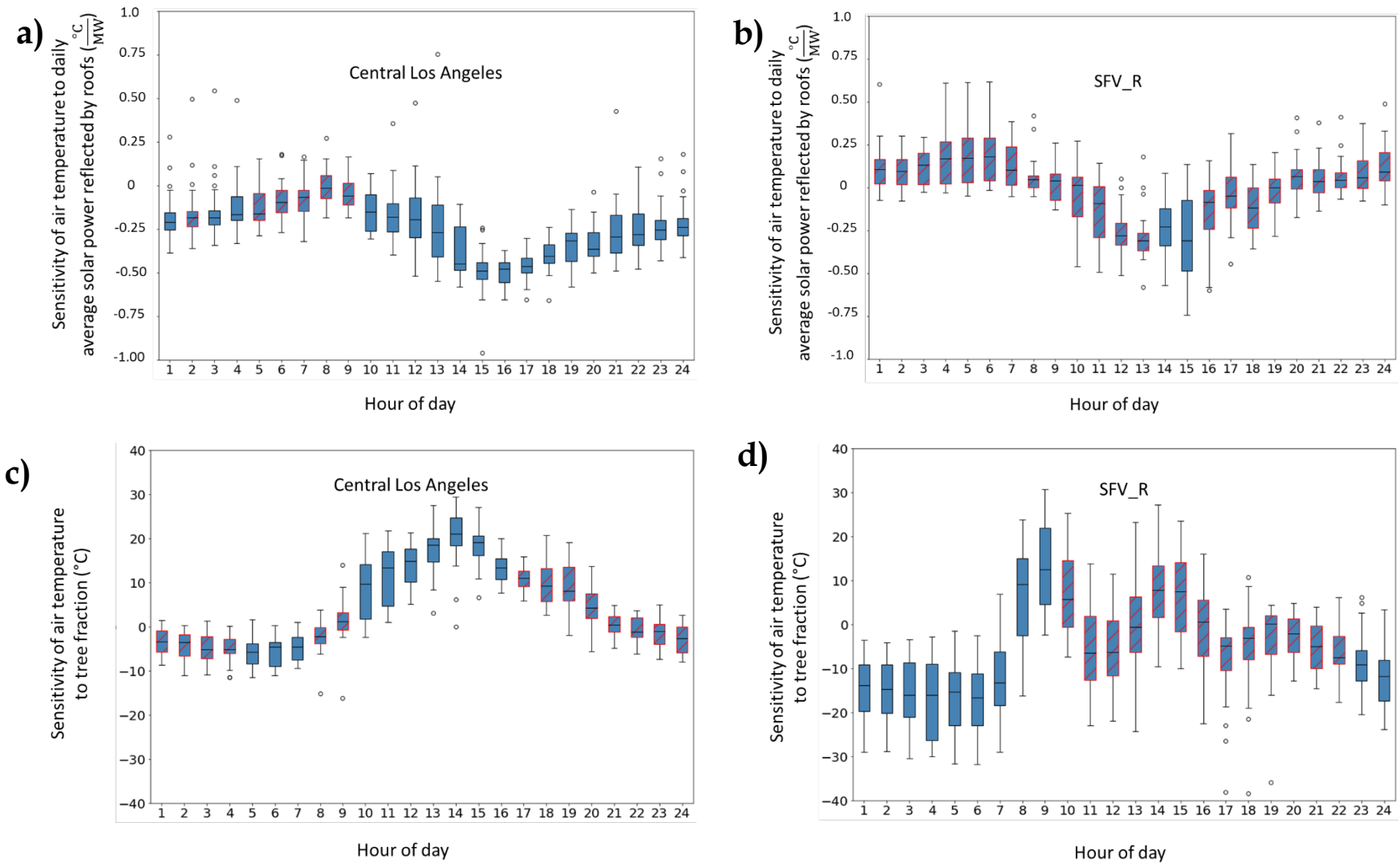

Figure 17. Boxplot for diurnal cycle of sensitivity of temperature to (a,b) daily average solar power reflected by roofs, and (c,d) tree fraction. Panels (a) and (c) are for Central Los Angeles and panels (b) and (d) are for SFV_R. Each box contains the sensitivities per hour for the entire month (July 2015). The hours with statistically insignificant sensitivities have red hatching. Boxes show the inner-quartile range, whiskers show the boundary of 1.5 interquartile range distance from first and third quartile, and the black line within the box represents the median. Hour of day 1 = 00:00 to 01:00 LDT.

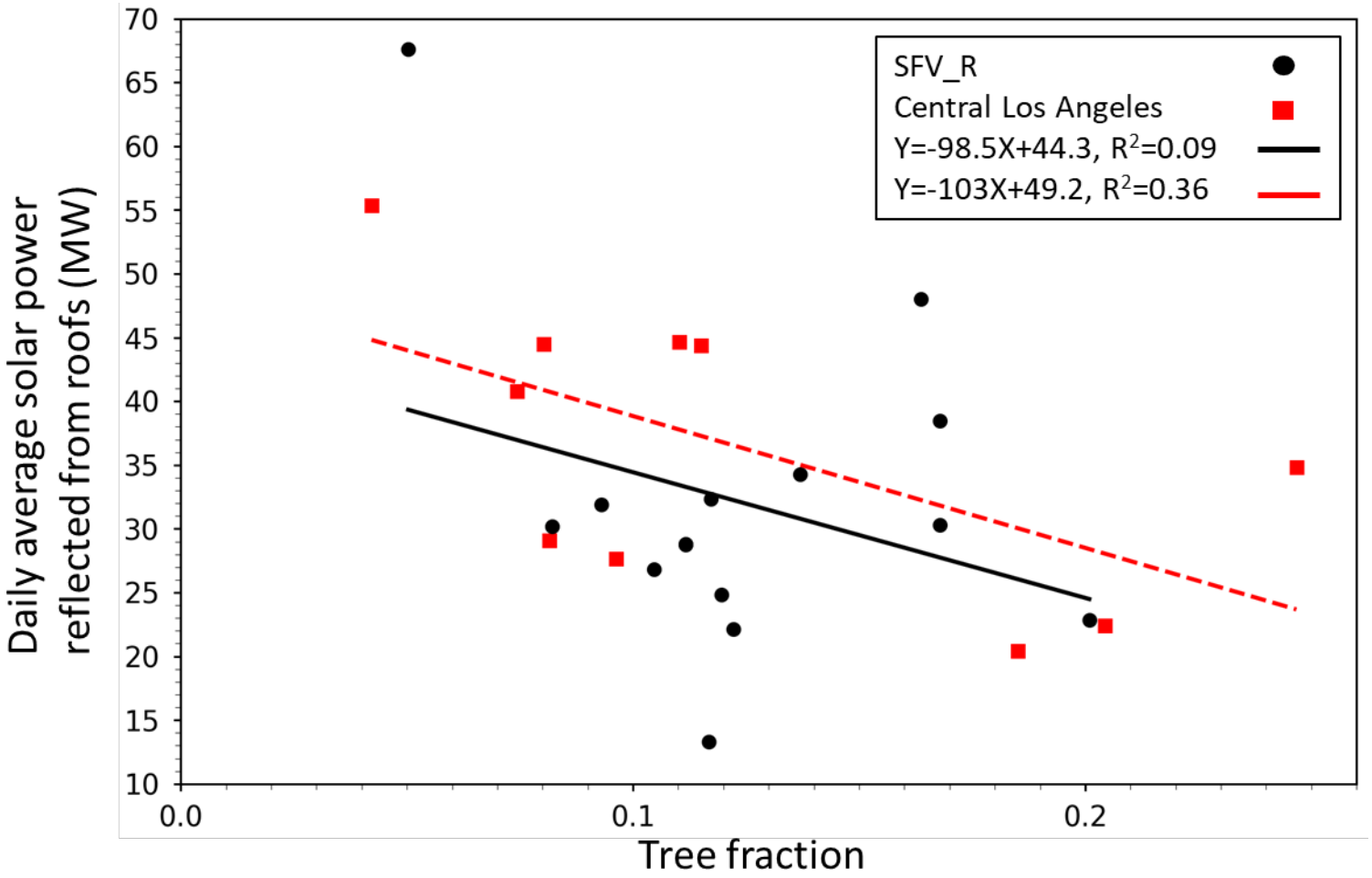

Figure 18. Daily average solar power reflected by roofs vs. tree fraction for each region. Each point represents a different neighborhood.

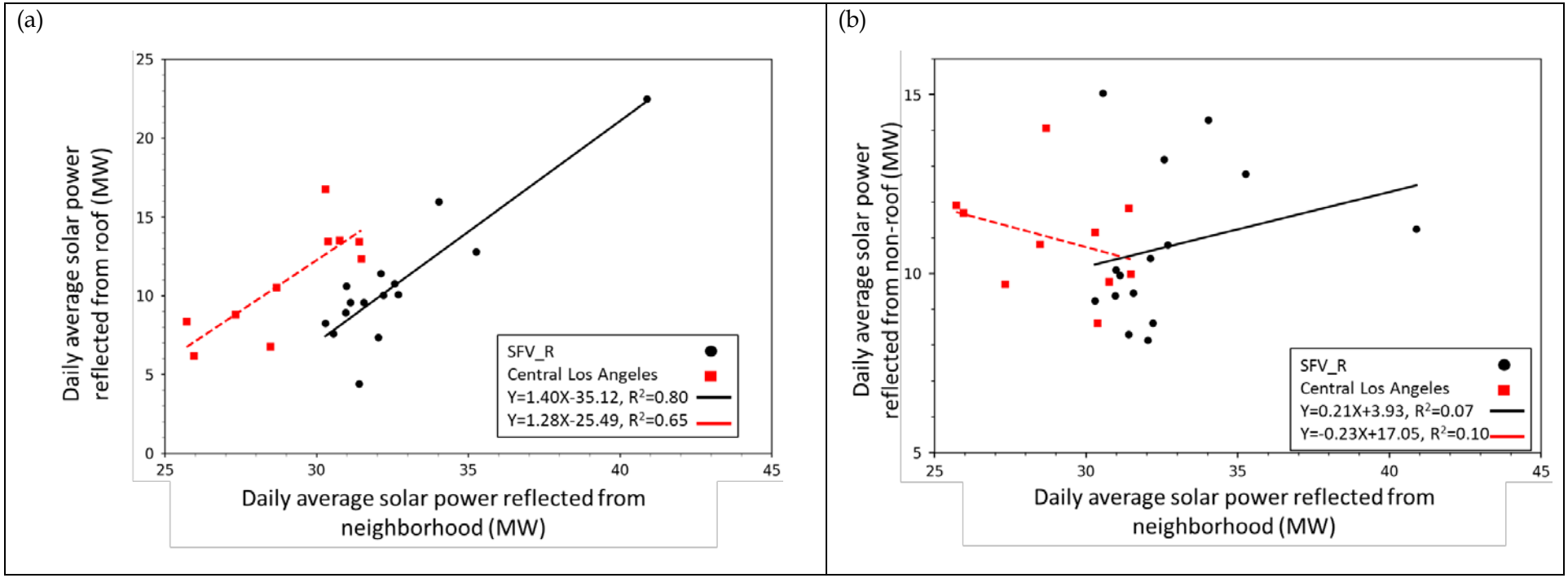

Figure 19. Comparison of daily average solar power reflected of (a) roofs and (b) non-roof surfaces to daily average solar power reflected from neighborhood. Least squares linear regressions are also shown separately for the two areas (i.e., SFV_R and Central Los Angeles). The higher coefficients of determination (R^2) in panel (a) versus (b) suggests that variations in roof albedo are responsible for the majority of variations in neighborhood albedo.

4.1.4 Utility of PWS Measurements

The PWS networks provided wider coverage of the LA Basin than other private or government operated networks. However, the data required extensive cleaning before it could be analyzed. Preprocessing the data was very time consuming but now we have clear steps to prepare other PWS data for future analysis.

4.2 Mobile Temperature Measurements

In this study, 15 different mobile-observation transects were carried out in 2016 and 2017 (Table 2). The mobile observations focused on the LA1 and SFV5 domains and were conducted on cloudless summer days and nights to capture the effects of LULC variations on temperature in urban areas.

4.2.1 Relation to LULC

Following model performance evaluation, correlations between observed temperature and surface physical properties were evaluated. In this case, two surface properties of interest were examined: (1) neighborhood-scale albedo and (2) vegetation canopy cover (500-m scale). We examined these two properties because they have been shown in many studies to have significant influence on the urban air temperature, and also because they are easy to control and deploy as mitigation measures. The relationships between observed air temperature (predictand) and either albedo and/or canopy cover (predictors) were examined in three manners: (1) simple linear regression, (2) multiple regression, and (3) CART analysis for further detail. Examples of each analysis are given in this discussion.

4.2.1.1 Simple linear regression

In the downtown Los Angeles (LA1) domain, observed air temperature from mobile transects was correlated to grid-level albedo and canopy cover. For the San Fernando Valley study area, the observed temperature was correlated only with canopy cover (as predictor) since albedo has a smaller variability in this domain (Figure 20). In this area, the roof albedos are generally higher than in other areas but there is smaller variability in albedo, from one roof to another, in this area compared to variability in other parts of the study domains.

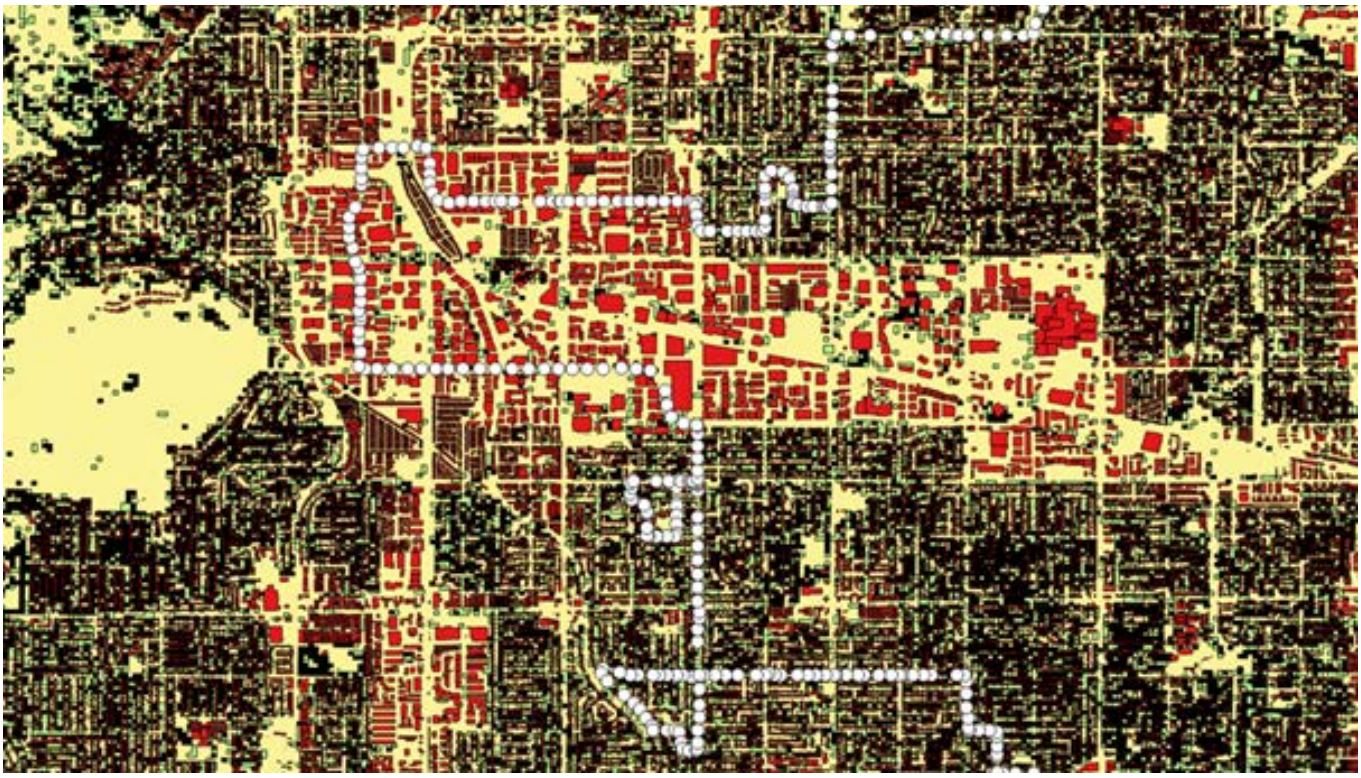

Figure 20. Detail from the San Fernando Valley study domain showing 30-m tree cover (yellow: < 10%, light green: 10 – 20%, black: > 20% cover), building-specific roof albedo (red: 0.05 – 0.25, orange: 0.25 – 0.50, light orange: 0.50 – 0.90), and a sample mobile transect segment (white dots).

The analysis summarized in Table 3 provides, for each transect segment, the temperature response to changes in albedo and/or canopy cover. These responses are computed as temperature change per 0.1 increase in albedo or canopy cover written symbolically as "$\Delta T / (\Delta a_{0.1})$" and "$\Delta T / (\Delta \eta_{0.1})$", respectively, along with the corresponding p-values (probability values). In this analysis, a significance level of 0.05 is selected and, as such, a p-value < 0.05 represents a statistically significant correlation between observed temperature (from the transect) and surface properties such as grid-level albedo and canopy cover (that were computed as input to the urbanized WRF model).

The results in Table 3 are based on a Cressman-weighting scheme (inverse distance) and a radius of influence of 1 km (from a mobile observation point to surrounding model grids), so that grid points within 500 m get the most weight and the ones at 1-km get a smaller weight. Transects TR01 – TR08, and TR13 are for LA1 and TR09-TR12, and TR15 are for the SFV5 study area.

Except for two entries in Table 3 (contribution of canopy cover to air temperature in transect TR01 and contribution of albedo to air temperature in transect TR02), all entries are statistically significant. For these two exception transects, the p-values suggest that in TR01, albedo is the main driver of air temperature and in TR02, canopy cover is the main driver.

In addition, all correlations are negative (i.e., when albedo and/or canopy cover increase, temperature decreases) except for transects TR02 (for canopy cover) and TR03 (for albedo). As discussed in the paper by Taha et al. (project paper), these two transects were among those carried out during periods of higher wind speeds which can weaken the correlations. In transects TR04 and TR05, the large temperature responses to albedo are likely because the transect temperature was measured on freeways and in an area with very extensive roof and pavement cover (> 95%), such that changes in albedo would have significant impacts.

Table 3. Summary of observed transect temperature response (°C) [°F] to changes in albedo and/or canopy cover (0.1 increase in albedo or canopy cover). Note that transects TR09 – TR15 have no entries in columns 3 and 4 because only canopy cover was considered in establishing correlations with air temperature.

Transect	Date / period	$\Delta T / (\Delta a_{0.1})$ (°C) [°F]	p-value	$\Delta T / (\Delta \eta_{0.1})$ (°C) [°F]	p-value
TR01	2017-06-14 day Part 1	-3.65 [-6.57]	< 0.0001	-0.10 [-0.18]	0.5300
TR02	2017-06-14 day Part 2	-1.04 [-1.87]	0.0817	0.65 [1.17]	0.0057
TR03	2017-06-14 day Part 3	1.00 [1.80]	0.0001	-0.40 [-0.72]	0.0074
TR04	2017-06-14 day Part 4	-14.70 [-26.46]	< 0.0001	-0.89 [-1.60]	0.0061
TR05	2017-08-28 day Part 1	-9.24 [-16.63]	< 0.0001	-2.20 [-3.96]	< 0.0001
TR06	2017-08-28 day Part 2	-1.10 [-1.98]	< 0.0001	-0.40 [-0.72]	< 0.0001
TR07	2017-08-28 night Part 1	-4.00 [-7.20]	< 0.0001	-1.61 [-2.89]	< 0.0001
TR08	2017-08-28 night Part 2	-3.40 [-6.12]	< 0.0001	-1.81 [-3.25]	< 0.0001
TR13	2016-04-22 day	-4.89 [-8.80]	< 0.0001	-0.22 [-0.39]	< 0.0001
TR09	2017-07-27 day Part 1			-0.40 [-0.72]	< 0.0001
TR10	2017-07-27 day Part 2			-0.11 [-0.19]	0.0105
TR11	2017-07-27 night Part 1			-0.20 [-0.36]	< 0.0001
TR12	2017-07-27 night Part 2			-1.06 [-1.91]	< 0.0001
TR15	2017-06-21 day			-0.53 [-0.95]	< 0.0001

4.2.1.2 Multiple regressions

Multiple regression was carried out for albedo and canopy cover as predictors to observed air temperature from the transects. This analysis applies only to the downtown area, LA1, since the San Fernando Valley analysis involved only variations in one predictor (canopy cover), because the variability in albedo is small.

The form of the correlation is given by Eq. (4) where a is albedo and η is canopy cover. The coefficients (C1, C2, C3) and corresponding p-values (p1, p2, p3) are given in Table 4. C1, C2, and C3 are in degrees C, and the "0.1" denominator simply indicates that the changes in temperature (C2 and C3) correspond to a 0.1 increase in surface albedo or a 0.1 increase in canopy cover.

$$T_{\text{air}} = C1 + \frac{C2}{0.1}\, a + \frac{C3}{0.1}\, \eta \qquad (4)$$

Table 4 summarizes the analysis at 1-km radii of influence using Cressman-type weighting. The results show that the correlations are overwhelmingly negative (as albedo and canopy cover increase, temperature decreases) and statistically significant except for three situations. These are in transect TR01, where the role of canopy cover is insignificant, and in transects TR02 and TR03, where the role of albedo is insignificant (as was discussed above).

Table 4. Eq. (4) applied to 1-km Cressman-type analysis of air temperature correlation to albedo and canopy cover.

Transect	*C1* (°C) [°F]	*p1*	*C2* (°C) [°F]	*p2*	*C3* (°C) [°F]	*p3*
TR01	33.25 [91.85]	< 0.0001	-3.70 [-6.66]	< 0.0001	-0.15 [-0.27]	0.3350
TR02	31.65 [88.97]	< 0.0001	-1.81 [-3.25]	0.1204	-1.08 [-1.94]	0.0154
TR03	29.42 [84.95]	< 0.0001	-0.15 [-0.27]	0.935	-0.75 [-1.35]	0.0086
TR04	47.18 [116.92]	< 0.0001	-13.95 [-25.11]	< 0.0001	-0.71 [-1.28]	0.0052
TR05	43.17 [109.70]	< 0.0001	-8.17 [-14.70]	< 0.0001	-1.97 [-3.54]	< 0.0001
TR06	33.25 [91.85]	< 0.0001	-0.78 [-1.40]	< 0.0001	-0.36 [-0.65]	< 0.0001
TR07	27.83 [50.09]	< 0.0001	-2.42 [-4.35]	< 0.0001	-1.47 [-2.64]	< 0.0001
TR08	30.04 [54.07]	< 0.0001	-3.71 [-6.67]	< 0.0001	-1.85 [-3.33]	< 0.0001
TR13	28.52 [51.33]	< 0.0001	-4.63 [-8.33]	< 0.0001	-0.10 [-0.18]	0.0500

4.2.1.3 Classification and regression tree

A classification and regression tree (CART) analysis was undertaken to assess the multiple interactions among predictors of mobile-observed air temperature. This additional analysis, discussed by Taha et al. (2018), was carried out for each transect—here, one example is presented. Essentially, this is an extension to the multiple regression analysis above and provides additional information. In the CART analysis, the roughness length parameter was introduced as an additional predictor to evaluate its role, if any, relative to that of albedo and canopy cover.

A CART is interpreted in the following manner: the variable above each node (circle) is a "splitting" variable, i.e., the criterion used in the correlation. The top splitting variable (i.e., the most important) is given above the top node. The yellow nodes are "terminal" nodes that show the final results (regression or classification) in which we are interested. At each node, there is a logical criterion: for values smaller than the criterion, follow the path to the left of the node. For values larger than the criterion, follow the path to the right. Each node is numbered (inside the circle). The number in italics below each node is the number of observational samples, and the number below that is the predicted value (in this case, air temperature) at the end of each path leading to a terminal node.

The example discussed here is for transect TR13 which is a daytime (13:00 LDT) transect in the downtown area (LA1) carried out on April 22, 2016. This transect segment consists of 798 temperature observations. The following can be deduced from this CART analysis (Figure 21):

In this transect segment, the most influential variable (top splitting node) is albedo.

Transect temperature readings are lower where albedo is larger. For grid-level albedo greater than 0.125, the temperatures are lowest, e.g., compare terminal nodes 6 and 7 (temperatures of 22.34 and 21.97 °C [72.21 and 71.54 °F]) with nodes 5, 9, 16, 34, and 35 (with higher temperatures of 22.90, 23.05, 23.17, 22.20, and 23.17 °C [73.22, 73.49, 73.70, 71.96, and 73.71 °F], respectively).

Calculating the weighted temperature differences for nodes with albedo higher then 0.125 (6 and 7) versus lower than 0.125 (nodes 5, 9, 16, 34, and 35), shows that the contribution of higher albedo in this transect is to lower air temperature by 0.81 °C (1.45 °F), which is significant.

Furthermore, within each subtree, the effects of increased albedo are also evident. For example, comparing terminal nodes 6 and 7 shows that readings where albedo is larger than 0.145 are 0.37 °C (0.66 °F) cooler than where albedo is lower than 0.145.

In this transect, where albedo is lower than 0.125, canopy cover also has a significant impact. Comparing node 5 (where canopy cover is greater than 0.195) and nodes 9, 16, 34, and 35 (where cover is lower than 0.195), the contribution of canopy cover is to cool the air by 0.12 °C (0.22 °F). This effect is relatively smaller than the effects of albedo in this transect.

Finally, the effects of roughness length are secondary and different from one subtree to another. For instance, whereas increased roughness length in node 35 relative to node 34 does show increased temperature, comparing the increased roughness in nodes 34 and 35 relative to node 16 shows the opposite effect.

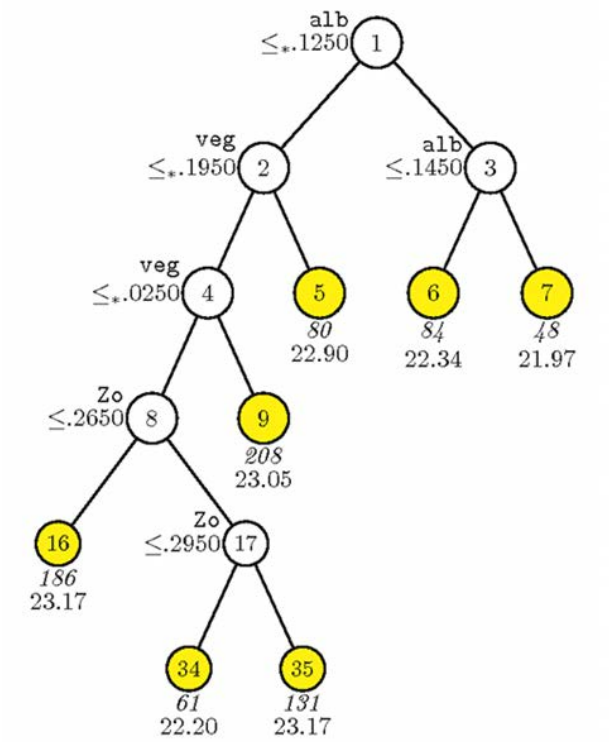

Figure 21. CART for transect TR13

4.3 Detection of Intra-urban Heat and Cool Islands

Because the Los Angeles region is one large urban-climate archipelago (a built-up area stretching from ocean to mountains), there is no rural reference against which the urban temperature is compared as in a "conventional" urban heat island definition. As such, our task was to identify intra-urban variations in heat and/or cool islands as a function of LULC (as an embedded signal) and correlate the temperature variations to changes in LULC and surface physical properties. As discussed above, our LULC analysis coupled with the fine-scale meteorological modeling result allowed us to identify such signals in the study areas as depicted in Figure 14.

The model performance evaluation in this study demonstrated that the WRF model and the modifications to its urban modules performed in this project can reproduce reasonably well the observations in the temperature, including the locations of UHI and UCI spots. As such, the model can be reliably applied to other urban areas and regions in California as well as for other applications such as in designing community- or neighborhood-scale UHI mitigation strategies

4.4 Performance and Utility of Mobile Monitors

The use of mobile transects was a very helpful component for our project. We were able to construct an affordable apparatus that could be installed on ride-share cars, which made the transects easy to conduct. The transect paths were designed to collect data in areas where there was no to minimal coverage by weather station networks. The mobile observations were very useful in validating the meteorological model performance.

5: Policy Implications and Lessons Learned

5.1 Lessons Learned

We envisioned installing 10+ stationary research-grade monitors in select locations to detect differences in air temperature from variations in LULC. However, the installation of stationary monitors proved more challenging than planned, while the mobile transects were easier than expected. Therefore, we installed fewer stationary monitors (four installed) than originally planned but completed 15 mobile transects to provide the observational data needed for our analysis.

We had strong institutional partners for this project in the LA Basin. Our plan was to use their facilities across the basin to site the stationary monitors. Since they were governmental organizations, we expected they would be able to make a long-term (5+ years) commitment to hosting the monitors and ensuring their security over time. However, we struggled to secure the many layers of approval needed to place monitors at facilities. We spent 18 months negotiating agreements, sites, and installation with partners. For future work, we would suggest allowing more time to negotiate all the approvals and/or include some financial agreement to ensure participation from individual facilities.

There were some beneficial changes we made from our project plan which aided implementation. For the mobile transects, we completed the first few transects using personal vehicles as planned. However, switching to the Uber ride-sharing service saved time and money by reducing both vehicle and staff costs. For future work, using ride-sharing services to help conduct mobile transects and measurements could be a good collaboration to take advantage of their large network of drivers and broad service area. Some of the ride-sharing fleet could be equipped with specialized sensors that track location and air temperatures across the city while the vehicles are in service.

5.2 Policy Implications

We found empirical evidence that there is intra-urban temperature variability correlated to LULC properties. The albedo and vegetation coverage values in our analysis are existing conditions in neighborhoods in LA where there has not been a concerted effort to mitigate UHIs. This suggests that there are opportunities for community cooling using existing technologies and practices to increase urban albedo and canopy cover. Knowing that these are effective cooling measures, cities can also accelerate the implementation of these UHI countermeasures in heat-vulnerable neighborhoods. Mitigating UHIs help locally offset future warming in cities from climate change. This will help the city build resiliency to future extreme heat events.

Local and state government policy makers can conduct similar modeling to identify local UHI areas to target policies to increase roof albedo and canopy cover. They can also review their city/community LULC datasets to identify areas where there is potential to increase roof albedo and vegetation cover. This will help them develop targeted strategies to implement UHI countermeasures. In turn, this can conserve city resources, program budgets, and staff, while also improving climate resiliency in the most heat-vulnerable communities. For example, the

City of Los Angeles' Department of Water and Power runs a residential cool roof rebate program. They can direct communication efforts to residential areas identified as local UHIs following the methodology of modeling used for this study. The installation of cool roofs in these UHI areas provide the neighborhood cooling benefit and building energy savings, while conserving program funds from city-wide outreach and implementation.

The California Natural Resources Agency also offers urban greening grants to cities, counties, and non-profits. Again, local or state agencies can review LULC datasets to target areas of low canopy coverage within disadvantaged communities for project implementation. If planted appropriately, trees could achieve the program objectives as well as providing the cooling benefit in heat-vulnerable communities.

6: Conclusions and Future Directions

6.1 Recommendations for Future Research

In this project, we found empirical evidence linking LULC to intra-urban air temperature variability. It leads us to several future research recommendations to validate our findings and to build upon these findings to help cities implement effective local UHI countermeasures:

- Repeat the personal weather station (PWS) analysis over the next few years as land cover properties evolve (e.g., increasing prevalence of cool roofs) and more PWS are added to networks.
- Repeat the PWS analysis using WeatherBug network data and measurements from the project's newly installed stationary monitors.
- Carry out additional transects, modeling, and analysis of PWS in other parts of Los Angeles Basin.
- Design a specialized air temperature sensor that piggybacks on ride-sharing vehicles to provide detailed time-and-space map of urban air temperature.
- Repeat the study for other areas in California.
- Complete related modeling and analysis for future-climate scenarios.
- Enhance analysis (observations, modeling, etc.) by including year-round conditions.
- Guide the implementation of cool-community measures by determining the minimum changes in albedo and vegetation cover (in heat-vulnerable communities) that are required to achieve cooling benefit.
- Establish a pilot community vulnerable to extreme heat to target the implementation of UHI countermeasures that will be modeled and monitored over time to measure their effectiveness in reducing community air temperatures.

6.2 Conclusions

Because California's urban heat islands are exacerbated by climate change in a manner that can compromise electricity sector resilience as well as public health, it is important to understand the factors that contribute to UHI as well as how UHI can be mitigated. In this study we carried out a multi-dimensional assessment of urban temperature variations based on state-of-the-science numerical modeling and several types of observations, including mobile transects and

personal weather stations. We sought to understand spatial air-temperature variations in local heat and cool islands and their relationship to land-use and land-cover properties in the Los Angeles Basin.

We collected detailed LULC datasets for the LA Basin that were used as inputs for the meteorological modeling and analysis. We also developed a database of historic micrometeorological information from existing weather station networks.

We partnered with the City of Los Angeles, County of Los Angeles, and Los Angeles Unified School District to help us find sites and hosts for stationary monitors in two study areas that we identified, San Fernando Valley and downtown Los Angeles (LA1). We used fine-resolution climate models to assess the potential UHI and/or UCI signals in these two areas. The results of the modeling informed the design of mobile-transect routes and siting of the stationary monitors. We designed a highly accurate and affordable stationary monitor that was installed in three locations in the SFV5 study area and at the University of Southern California campus west of downtown Los Angeles. To supplement the data collected from the stationary monitors, we completed 15 mobile transects. We designed and constructed an apparatus that is easily mounted on the roof of a car to measure air temperature along the transect routes.

We assessed data from PWS in the Weather Underground network to relate observed intra-urban temperature variations to LULC and surface physical properties. We also analyzed observational micrometeorological data from mobile transects and correlated it with neighborhood-scale albedo and vegetation canopy cover.

We found the first observational evidence from analysis of high spatial density weather stations that increases in roof albedo at neighborhood scale are associated with reductions in near-surface air temperature. This was corroborated with the analysis from mobile transect measurements, which revealed a cooling effect from area-wide increase in albedo and/or canopy cover. The albedo and canopy cover values in our analysis are existing conditions in neighborhoods in LA where there has not been a concerted effort to mitigate UHIs. This suggests that there are opportunities for community cooling using existing technologies and practices to increase urban albedo and canopy cover. Knowing that these are effective cooling measures, cities can also accelerate the implementation of these UHI countermeasures in heat-vulnerable neighborhoods.

In addition, the calibrated meteorological model was able to accurately identify the localized urban heat islands and urban cool islands observed in this study. Therefore, it can be applied by stakeholders, including city and state government, to characterize the intra-urban microclimate variations elsewhere in California, and they can also apply the model to analyze the benefits from deploying UHI countermeasures.

7: References

Akbari H, Rose S, Taha H. 1999. Characterizing the fabric of the urban environment: A case study of Sacramento, California. Report LBNL-44688, Lawrence Berkeley National Laboratory, Berkeley, CA. https://doi.org/10.2172/764362

Alexander PG, Mills G. 2014. Local climate classification and Dublin's urban heat island. *Atmosphere* 5, 755-774, https://doi.org/10.3390/atmos5040755

Anderson JR, Hardy EE, Roach JT, Witmer RE. 2001. A land use and land cover classification system for use with remote sensor data. USGS Professional Paper 964, U.S. Government Printing Office, Washington, DC. http://pubs.er.usgs.gov/publication/pp964

Arya SP. 1988. *Introduction to Micrometeorology*. San Diego: Academic Press.

Ban-Weiss GA, Woods J, Levinson R. 2015. Using remote sensing to quantify albedo of roofs in seven California cities, Part 1: Methods. *Solar Energy* 115, 777-790, https://doi.org/10.1016/j.solener.2014.10.022

Ban-Weiss GA, Woods J, Millstein D, Levinson R. 2015. Using remote sensing to quantify albedo of roofs in seven California cities, Part 2: Results and application to climate modeling. *Solar Energy* 115, 791-80, https://doi.org/10.1016/j.solener.2014.10.041

Bjorkman J, Thorne JH, Hollander A, Roth NE, Boynton RM, de Goede J, Xiao Q, Beardsley K, McPherson G, Quinn JF. 2015. Biomass, carbon sequestration and avoided emission: assessing the role of urban trees in California. Information Center for the Environment, University of California, Davis. https://escholarship.org/uc/item/8r83z5wb

Bruse M, Fleer H. 1998. Simulating surface–plant–air interactions inside urban environments with a three dimensional numerical model. *Environmental Modelling & Software*, 13, 373-384. https://doi.org/10.1016/S1364-8152(98)00042-5

Burian SJ, Han WS, Velugubantla SP, Maddula SRK. 2003. Development of gridded fields of urban canopy parameters for Models-3/CMAQ/MM5. Department of Civil and Environmental Engineering, University of Utah.

Cal-Adapt, 2018. Extreme Heat Days & Warm Nights. Developed by University of California Berkeley's Geospatial Innovation Facility for California Energy Commission. Accessed 3 May 2018 at http://cal-adapt.org/tools/extreme-heat/

CAMS 2011. LA County Street & Address File. https://egis3.lacounty.gov/dataportal/2014/06/16/2011-la-county-street-centerline-street-address-file/ (accessed November 2016)

CARB 2017. Life-Cycle Assessment and Co-Benefits of Cool Pavements. https://www.arb.ca.gov/research/apr/past/12-314.pdf

Chen F, Kusaka H, Bornstein R, Ching J, Grimmond CSB, Grossman-Clarke S, Loridan T, Manning K, Martilli A, Miao S, Sailor D, Salamanca F, Taha H, Tewari M, Wang X, Wyszogrodzki A, Zhang C. 2010. The integrated WRF/urban modeling system:

development, evaluation, and applications to urban environmental problems. *International Journal of Climatology* 31, 273-288. https://doi.org/10.1002/joc.2158.

Cheng H, Castro IP. 2002. Near-wall flow over urban-like roughness. *Boundary-Layer Meteorology* 104, 229-259. https://doi.org/10.1023/A:1016060103448

Ching J, Brown M, Burian S, Chen F, Cionco R, Hanna A, Hultgren T, McPherson T, Sailor D, Taha H, Williams D. 2009. National urban database and access portal tool, NUDAPT. Bulletin of the American Meteorological Society, https://doi.org/10.1175/2009BAMS2675.1.

Ellis KN, Hathaway L, Mason R, Howe DA, Epps TH, Brown VM. 2015. Summer temperature variability across four urban neighborhoods in Knoxville, Tennessee, USA. *Theoretical and Applied Climatology* 127, 701-710. https://doi.org/10.1007/s00704-015-1659-8

Georgakis C, Santamouris M. 2017. Determination of the surface and canopy urban heat island in Athens central zone using advanced monitoring. *Climate* 5, 97 (13 pp), https://doi.org/10.3390/cli5040097

ENVI_MET, 2018. Local air quality and weather simulation model. http://www.envi-met.com

Gershunov A, Cayan DR, Iacobellis SF. 2009. The great 2006 heat wave over California and Nevada: Signal of an increasing trend. *Journal of Climate* 22, 6181-6203. https://doi.org/10.1175/2009JCLI2465.1

Hamada S, Oht, T. 2010. Seasonal variations in the cooling effect of urban green areas on surrounding urban areas. *Urban Forestry and Urban Greening*, 9, 15-24. https://doi.org/10.1016/j.ufug.2009.10.002

Herbel I, Croitoru A-E, Rus I, Harpa GV, Ciupertea A-F. 2016. Detection of atmospheric urban heat island through direct measurements in Cluj-Napoca City, Romania. *Hungarian Geographical Bulletin* 2, 117-128. https://doi.org/10.15201/hungeobull.65.2.3

Jin H, Cui P, Wong NH, Ignatius M. 2018. Assessing the effects of urban morphology parameters on microclimate in Singapore to control the urban heat island effect. *Sustainability* 10, 206. https://doi.org/10.3390/su10010206

Jonsson P. 2004. Vegetation as an urban climate control in the subtropical city of Gaborone, Botswana. *International Journal of Climatology* 24, 1307-1322, https://doi.org/10.1002/joc.1064

Kistler R, Kalnay E, Collins W, et al.. 2001. The NCEP-NCAR 50-year reanalysis: Monthly means CDROM and documentation. *Bulletin of the American Meteorological Society* 82, 247-267. https://doi.org/10.1175/1520-0477(2001)082%3C0247:TNNYRM%3E2.3.CO;2

Kusaka H, Kondo H, Kikegawa Y, Kimura F. 2001. A simple single-layer urban canopy model for atmospheric models: Comparison with multi-layer and slab models. Boundary-Layer Meteorology 101, 329-358. https://doi.org/10.1023/A:1019207923078

Levinson R, Taha H, Mohegh A, Gilbert H, Ban-Weiss G, Chen S. 2018. Monitoring the urban heat island effect and the efficacy of future countermeasures. California Energy

Commission. Final report for research supported under Energy Commission grant no. EPC-14-073.

Los Angeles Region Imagery Acquisition Consortium (LAR-IAC) 2008. County Wide Building Outlines, http://egis3.lacounty.gov/dataportal/2011/04/28/countywide-building-outlines/

Macdonald RW, Griffiths RF, Hall DJ. 1998. An improved method for estimation of surface roughness of obstacle arrays. *Atmospheric Environment* 32, 1857–1864. https://doi.org/10.1016/S1352-2310(97)00403-2

Martilli A, Clappier A, Rotach MW. 2002. An urban surface exchange parameterization for mesoscale models. *Boundary-Layer Meteorology* 104, 261-304. https://doi.org/10.1023/A:1016099921195

Masson V. 2000. A physically-based scheme for the urban energy budget in atmospheric models. *Boundary-Layer Meteorology* 94 357-397. https://doi.org/10.1023/A:1002463829265

Multi-Resolution Land-Characteristics Consortium (MRLC) 2014. National Land Cover Databases. http://www.mrlc.gov/nlcd2006.php

NOAA. 2016. Land-based station data. National Centers for Environmental Information (formerly National Climatic Data Center), National Oceanic and Atmospheric Administration. https://www.ncdc.noaa.gov/data-access/land-based-station-data (accessed Sep 2016)

Panofsky HA, Dutton JA. 1984. *Atmospheric Turbulence: Models and Methods for Engineering Applications*. John Wiley & Sons, New York, 397 pp.

Pleim J, Xiu A, Finkelstein P, Otte T. 2001. A coupled land-surface and dry deposition model and comparison to field measurements of surface heat, moisture, and ozone fluxes. *Water, Air, and Soil Pollution* 1, 243-252. https://doi.org/10.1023/A:1013123725860

Pomerantz M, Pon B, Akbari H, Chang SC. 2000. The effect of pavements' temperatures on air temperatures in large cities. Report LBNL-43442, Lawrence Berkeley National Laboratory, Berkeley, CA. Retrieved 2015-12-10 from https://heatisland.lbl.gov/publications/effect-pavements-temperatures-air .

Qiu GY, Zou Z, Li X, Li H, Guo Q, Yan C, Tan S. 2017. Experimental studies on the effects of green space and evapotranspiration on urban heat island in a subtropical megacity in China. *Habitat International* 68, 30-42. https://doi.org/10.1016/j.habitatint.2017.07.009

Rose S, Akbari H, Taha H. 2003. Characterizing the fabric of the urban environment: A case study of Greater Houston, Texas. Report LBNL-51448, Lawrence Berkeley National Laboratory, Berkeley, CA. https://www.osti.gov/servlets/purl/816533

Sakakibara Y. 1996. A numerical study of the effect of urban geometry upon the surface energy budget. *Atmospheric Environment* 30, 487-496. https://doi.org/10.1016/1352-2310(94)00150-2

Santamouris M. 2014. Cooling the cities - A review of reflective and green roof mitigation technologies to fight heat island and improve comfort in urban environments. *Solar Energy* 103, 682-703. https://doi.org/10.1016/j.solener.2012.07.003

Simpson J, McPherson G. 2007. Preliminary evaluation of the potential air quality benefits of trees within SIP guidelines. Center for Urban Forest Research, PSW, USDA Forest Service (May 2007).

Skamarock W, Klemp J, Dudhia J, et al. 2008. A description of the Advanced Research WRF. NCAR Technical Note NCAR/TN-475+STR, National Center for Atmospheric Research, Boulder, Colorado. http://dx.doi.org/10.5065/D68S4MVH

Southern California Association of Governments (SCAG) 2012. SCAG 2012 Land Use. http://egis3.lacounty.gov/dataportal/2012/04/10/countywide-zoning/

Stewart ID, Oke TR. 2012. Local climate zones for urban temperature studies. *Bulletin of the American Meteorological Societ*y 93(12), 1879-1900. https://doi.org/10.1175/BAMS-D-11-00019.1

Sun C-Y, Brazel AJ, Chow WTL, Hedquist BC, Prashad L. 2009. Desert heat island study by mobile transect and remote sensing techniques. *Theoretical and Applied Climatology* 98, 323-335, https://doi.org/10.1007/s00704-009-0120-2

Taha H. 1997. Urban climates and heat islands: Albedo, evapotranspiration, and anthropogenic heat. *Energy & Buildings* 25, 99-103. https://doi.org/10.1016/S0378-7788(96)00999-1

Taha H. 2007. Urban surface modification as a potential ozone air-quality improvement strategy in California -- Phase 2: Fine-resolution meteorological and photochemical modeling of urban heat islands. Final report prepared by Altostratus Inc. for the California Energy Commission, Sacramento, California, PIER Environmental Research. http://www.energy.ca.gov/2009publications/CEC-500-2009-071/CEC-500-2009-071.PDF

Taha H. 2008a. Meso-urban meteorological and photochemical modeling of heat island mitigation. *Atmospheric Environment* 42, 8795–8809. https://doi.org/10.1016/j.atmosenv.2008.06.036.

Taha H. 2008b. Episodic performance and sensitivity of the urbanized MM5 (uMM5) to perturbations in surface properties in Houston TX. *Boundary-Layer Meteorology* 127, 193-218. https://doi.org/10.1007/s10546-007-9258-6.

Taha H. 2008c. Urban surface modification as a potential ozone air-quality improvement strategy in California: A mesoscale modeling study. *Boundary-Layer Meteorology* 127, 219-239. https://doi.org/10.1007/s10546-007-9259-5.

Taha H. 2013. Meteorological, emissions, and air-quality modeling of heat-island mitigation: Recent findings for California, U.S.A. *International Journal of Low Carbon Technologies* 10, 3-14, https://doi.org/10.1093/ijlct/ctt010

Taha H. 2015. Cool cities: counteracting potential climate change and its health impacts. Invited paper, *Current Climate Change Reports* 1, 163-175. https://doi.org/10.1007/s40641-015-0019-1.

Taha H. 2017. Characterization of urban heat and exacerbation: Development of a heat island index for California. *Climate* 5, 59, https://doi.org/10.3390/cli5030059

Taha H, Freed T. 2015. Creating and mapping an urban heat island index for California. Final report prepared by Altostratus Inc. for the California Environmental Protection Agency (Cal/EPA) under Contract 13-001. The study report is available on the Cal/EPA web site at: http://www.calepa.ca.gov/UrbanHeat/Report/Report.pdf. The Cal/EPA website for the data and the interactive maps is at: http://www.calepa.ca.gov/UrbanHeat/Maps/default.htm.

Taha H, Levinson R, Mohegh A, Gilbert H, Ban-Weiss G, Chen S. 2018. Air-temperature response to neighborhood-scale variations in albedo and canopy cover in the real world: Fine-resolution meteorological modeling and mobile temperature observations in the Los Angeles climate archipelago. *Climate* 6, 53 (25 pp). https://doi.org/10.3390/cli6020053

Taha H, Wilkinson J, Bornstein R, Xiao Q, McPherson G, Simpson J, Anderson C, Lau S, Lam J, Blain C. 2015. An urban–forest control measure for ozone in the Sacramento, CA Federal Non-Attainment Area (SFNA). *Sustainable Cities and Society* 21, 51-65. https://doi,org/10.1016/j.scs.2015.11.004

Tesche TW, McNally DE, Emery CA, Tai E. 2001. Evaluation of the MM5 model over the Midwestern U.S. for three 8-hour oxidant episodes, Prepared for the Kansas City Ozone Technical Workgroup. Alpine Geophysics LLC and Environ Corp.

Tsin PK, Knudby A, Krayenhoff ES, Ho HC, Brauer M, Henderson SB. 2016. Microscale mobile monitoring of urban air temperature. *Urban Climate* 18, 58-72, https://doi.org/10.1016/j.uclim.2016.10.001

Vahmani P, Ban-Weiss GA. 2016. Impact of remotely sensed albedo and vegetation fraction on simulation of urban climate in WRF-urban canopy model: A case study of the urban heat island in Los Angeles. *Journal of Geophysical Research* 121, 1511–1531. https://doi.org/10.1002/ 2015JD023718.

Voogt JA, Oke TR. 1998. Effects of urban surface geometry on remotely-sensed surface temperature. International Journal of Remote Sensing, 19, 895– 920.

Weather Underground 2016. Weather Underground API. https://www.wunderground.com/weather/api/ (accessed September 2016).

Weng Q, Quattrochi DA. 2006. Thermal remote sensing of urban areas: An introduction to the special issue. *Remote Sensing of Environment* 104, 119-122. https://doi.org/10.1080/014311698215784

Weng, Qihao. 2009. Thermal infrared remote sensing for urban climate and environmental studies: Methods, applications, and trends. *ISPRS Journal of Photogrammetry and Remote Sensing* 64, 335-344. https://doi.org/10.1016/j.isprsjprs.2009.03.007.

World Meteorological Organization. 2006. Initial guidance to obtain representative meteorological observations at urban sites (TR Oke). WMO Report No. 81, WMO/TD-No. 1250. http://library.wmo.int/pmb_ged/wmo-td_1250.pdf